

# Polycomb-like proteins link the PRC2 complex to CpG islands

Haojie Li<sup>1\*</sup>, Robert Liefke<sup>2,3\*</sup>, Junyi Jiang<sup>1\*</sup>, Jesse Vigoda Kurland<sup>4</sup>, Wei Tian<sup>1</sup>, Pujan Deng<sup>1</sup>, Weidi Zhang<sup>1</sup>, Qian He<sup>1</sup>, Dinshaw J. Patel<sup>5</sup>, Martha L. Bulyk<sup>4,6</sup>, Yang Shi<sup>2,3</sup> & Zhanxin Wang<sup>1</sup>

The Polycomb repressive complex 2 (PRC2) mainly mediates transcriptional repression<sup>1,2</sup> and has essential roles in various biological processes including the maintenance of cell identity and proper differentiation. Polycomb-like (PCL) proteins, such as PHF1, MTF2 and PHF19, are PRC2-associated factors that form sub-complexes with PRC2 core components<sup>3</sup>, and have been proposed to modulate the enzymatic activity of PRC2 or the recruitment of PRC2 to specific genomic loci<sup>4–13</sup>. Mammalian PRC2-binding sites are enriched in CG content, which correlates with CpG islands that display a low level of DNA methylation<sup>14</sup>. However, the mechanism of PRC2 recruitment to CpG islands is not fully understood. Here we solve the crystal structures of the N-terminal domains of PHF1 and MTF2 with bound CpG-containing DNAs in the presence of H3K36me3-containing histone peptides. We show that the extended homologous regions of both proteins fold into a winged-helix structure, which specifically binds to the unmethylated CpG motif but in a completely different manner from the canonical winged-helix DNA recognition motif. We also show that the PCL extended homologous domains are required for efficient recruitment of PRC2 to CpG island-containing promoters in mouse embryonic stem cells. Our research provides the first, to our knowledge, direct evidence to demonstrate that PCL proteins are crucial for PRC2 recruitment to CpG islands, and further clarifies the roles of these proteins in transcriptional regulation *in vivo*.

PHF1, MTF2 and PHF19 (also known as PCL1, PCL2 and PCL3, respectively) are mammalian Polycomb-like proteins that interact with PRC2 directly<sup>4,5</sup>. All three possess a Tudor domain, two plant homeodomain (PHD) fingers, an extended homologous (EH) region clustered at the N terminus, and a chromo-like domain located at the C terminus (Fig. 1a, Extended Data Fig. 1a). Currently, only the structures of the isolated Tudor domains of PCL proteins have been solved, and these bind preferentially to histone H3 trimethylated at lysine 36 (H3K36me3)<sup>4,6,7,11,15,16</sup>. We solved the crystal structure of the PHF1 Tudor–PHD1–PHD2–EH cassette at 1.9 Å resolution (Extended Data Table 1). In the apo-form structure, these four domains organize into a compact upside-down triangle plus a handle architecture, with the Tudor, PHD1 and PHD2 domains forming the triangular head and the EH domain forming the handle (Fig. 1b). The Tudor and both PHDs have close contacts with one another, while the EH domain contacts only PHD2.

The PHF1 EH region folds into a domain containing three  $\alpha$ -helices and a curved three-stranded  $\beta$ -sheet. A structure-based homology search using the Dali server<sup>17</sup> demonstrated that it resembles a series of winged-helix motifs as proposed<sup>18</sup>. Comparison with the typical winged-helix motif of HNF-3 $\gamma$  (also known as FOXA3)<sup>19</sup> showed that

the major structural elements are well superimposed, while large structural variations occur mainly at the wing-like loops (W1 and W2) and the loop between helix 2 and helix 3 (Fig. 1c).

Given that the winged-helix motif is the defining DNA-binding domain of a family of forkhead transcription factors<sup>19</sup>, we speculated that PHF1 may also target specific DNA elements through its winged-helix motif in the EH region (EH<sub>WH</sub>). Using an electrophoretic mobility shift assay (EMSA), we found that PHF1 neither binds DNA containing the consensus sequence (5'-GTAAACAA-3') recognized by several

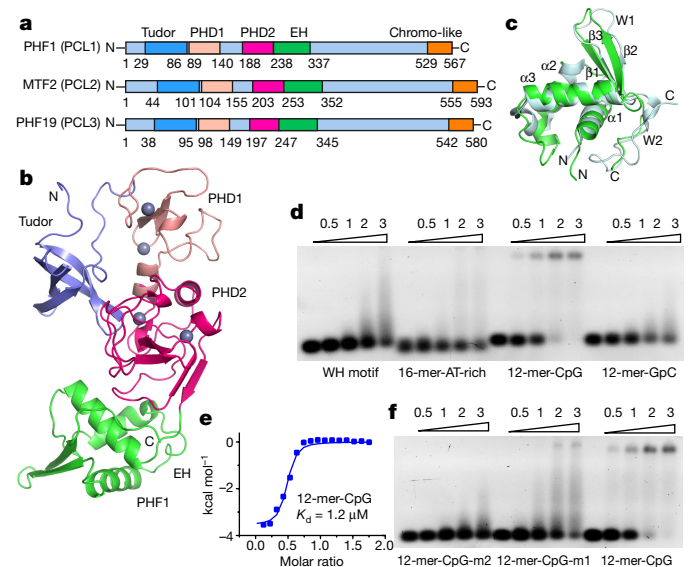


**Figure 1 | PHF1 domain architecture, its free form structure and the binding analysis with various double-stranded DNAs. a**, Domain architecture of human PCL proteins. **b**, Free-form structure of the PHF1 Tudor–PHD1–PHD2–EH cassette. The Tudor, PHD1, PHD2 and EH domains were coloured in blue, salmon, magenta and green, respectively. Zinc ions are shown as grey balls. **c**, Overlapped structures of the PHF1 EH domain coloured in green and the HNF-3 $\gamma$  winged-helix motif coloured in cyan, with a root mean squared deviation (r.m.s.d.) value of around 2.3 Å over 66 equivalent protein backbone atoms. **d**, EMSA results of the PHF1 cassette with different double-stranded DNAs. Protein-to-DNA molar ratios are shown at the top. WH, winged helix. **e**, ITC-based measurement of the PHF1 cassette with the 12-mer-CpG DNA. **f**, EMSA analysis of the PHF1 cassette with hemi-methylated or fully methylated 12-mer-CpG DNAs. Protein-to-DNA molar ratios are indicated at the top. EMSA and ITC data are representative of at least three independent experiments. Uncropped gels are shown in Supplementary Fig. 1.

<sup>1</sup>Key Laboratory of Cell Proliferation and Regulation Biology of Ministry of Education, College of Life Sciences, Beijing Normal University, 19 Xijiekouwai Avenue, Beijing 100875, China. <sup>2</sup>Division of Newborn Medicine and Epigenetics Program, Department of Medicine, Boston Children's Hospital, Boston, Massachusetts 02115, USA. <sup>3</sup>Department of Cell Biology, Harvard Medical School, Boston, Massachusetts 02115, USA. <sup>4</sup>Division of Genetics, Department of Medicine, Brigham and Women's Hospital and Harvard Medical School, Boston, Massachusetts 02115, USA. <sup>5</sup>Structural Biology Program, Memorial Sloan-Kettering Cancer Center, New York, New York 10065, USA. <sup>6</sup>Department of Pathology, Brigham and Women's Hospital and Harvard Medical School, Boston, Massachusetts 02115, USA.

\*These authors contributed equally to this work.

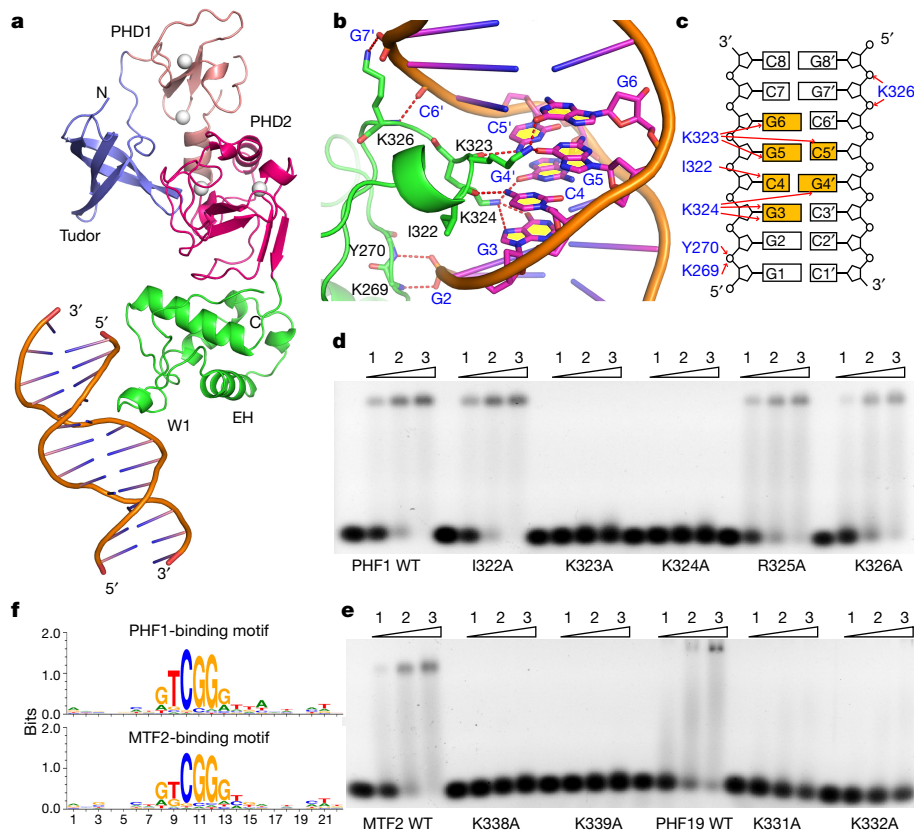


**Figure 2 | Structural details of PHF1 with bound DNA, mutational analysis of the PCL cassettes, and identification of DNA motifs recognized by PHF1 and MTF2 through protein-binding microarrays.** **a**, Overall structure of the PHF1 cassette with bound DNA. **b**, Detailed interactions of the PHF1 EH domain with bound DNA. The PHF1 EH domain is coloured in green. Hydrogen bonds are shown as red dotted lines. **c**, Schematic representation of PHF1–DNA interactions. **d**, **e**, EMSA results of the binding of 12-mer-CpG DNA with wild-type (WT) or

mutant forms of PHF1 (**d**), MTF2 and PHF19 (**e**). Protein-to-DNA molar ratios are shown at the top. **f**, DNA-binding specificity motifs recognized by the PHF1 and MTF2 PHD2–EH fragments identified from universal protein-binding microarrays using the Universal PBM Analysis Suite<sup>28</sup>. Information content (bits) is on the y axis, and position is on the x axis. Data are representative of two independent experiments. Uncropped gels are shown in Supplementary Fig. 1.

FOX family members<sup>20</sup>, nor binds AT-rich DNA fragments (Fig. 1d). By contrast, the PHF1 cassette binds a 12-base-pair CG-rich DNA with the palindromic sequence 5'-GGGCGGCCGCC-3' containing 2 CpG motifs (referred to as 12-mer-CpG, Fig. 1d). Isothermal titration calorimetry (ITC)-based measurements demonstrated that PHF1 binds the 12-mer-CpG DNA with a dissociation constant ( $K_d$ ) value of around 1.2  $\mu$ M and a molar ratio of around 2:1 (Fig. 1e and Extended Data Table 2). Changing the sequence to 5'-GGGGGGCCCC-3' that loses both CpG motifs but retains a GpC motif abolishes the binding for PHF1 completely (Fig. 1d), suggesting that it is the CpG motif, but not the GpC motif, that is required for binding. Consistently, all the DNAs tested without CpG motifs fail to bind the PHF1 cassette (Extended Data Fig. 2a and Extended Data Table 3). In vertebrates, the CpG motif is a frequent target of DNA methylation, resulting in hemi- or fully methylated substrates<sup>21</sup>. The PHF1 cassette shows reduced binding for the hemi-methylated 12-mer-CpG DNA and a loss of binding for the fully methylated substrate (Fig. 1f). Taken together, we conclude that PHF1 EH<sub>WH</sub> preferentially binds unmethylated CpG-containing DNA substrates.

We solved the crystal structure of the binary complex of the PHF1 cassette bound to the 12-mer-CpG DNA with a 3'-overhanging thymine (Fig. 2a and Extended Data Table 1). The DNA is recognized mainly through the W1 loop located on a positively charged surface of the EH<sub>WH</sub> (Extended Data Fig. 3a). The W1 loop penetrates into the CpG-containing major groove, with the 322-Ile-Lys-Lys-324 tripeptide forming extensive intermolecular contacts with both cytosine and guanine residues of a CpG duplex, thus contributing to the CpG selectivity (Fig. 2b, c). Bases C4 and C5', the symmetrically related

cytosines of a CpG duplex, are anchored in place by forming a hydrogen bond each with the main-chain carbonyl oxygen atoms of Ile322 and Lys323, respectively. Their complementary guanines, G4' and G5, are each stabilized through a hydrogen bond with the side chains of Lys324 and Lys323, respectively. Methylation of either cytosine, or replacing the cytosine residues of the CpG segment with other bases, would disrupt these intermolecular hydrogen bonds, or cause steric clashes with the protein backbone. In addition, G3 and G6, the bases flanking the CpG dinucleotide, form additional hydrogen bonds with the side chains of Lys324 and Lys323, respectively, which further stabilizes the recognition and may account for the preference for flanking bases (Fig. 2b, c). Besides the above base-specific recognition, Lys326 interacts with the backbone phosphate from both G7' and C6' through hydrogen bonding; Lys269 and Tyr270, located on the  $\beta$ 1 strand of the EH<sub>WH</sub>, each interact with the backbone phosphate of G2 through main-chain hydrogen bonding. Overall, the EH<sub>WH</sub> targets the CpG-containing major groove over a 6-base-pair footprint, while bases from the minor groove are not targeted (Fig. 2c). Owing to the insertion of the W1 loop, the major groove of the bound DNA is distorted and 2.5 Å wider than that of a canonical B-form DNA (Extended Data Fig. 3b). Lys323 and Lys324 in the W1 loop have central roles in recognizing the CpG motif, as both the Lys323Ala and the Lys324Ala mutants show a complete loss of binding (Fig. 2d). By contrast, the Ile322Ala, Arg325Ala and Lys326Ala mutations do not or only modestly affect the binding affinity (Fig. 2d). The W1 loop-mediated DNA-recognizing mechanism of PHF1 EH<sub>WH</sub> is different from other known winged-helix motifs, among which the HNF-3 $\gamma$  winged-helix motif recognizes DNA mainly through the third  $\alpha$ -helix<sup>19</sup>, while the hRFX1

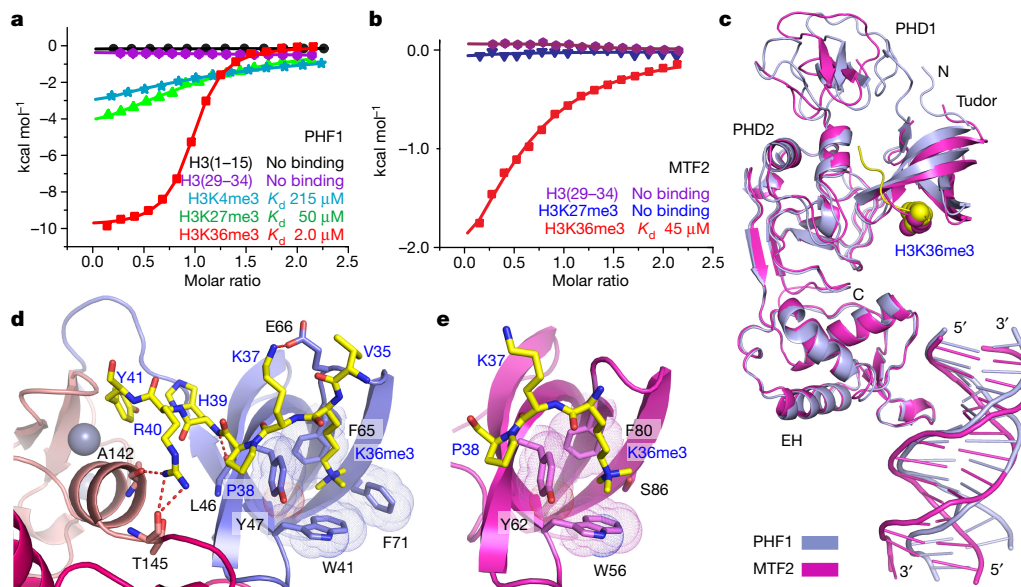


**Figure 3 | Binding analysis of the PHF1 and MTF2 cassettes with various histone peptides and structural details of PHF1/MTF2 cassette-H3K36me3-DNA ternary complexes.** **a, b**, ITC-based measurements of the PHF1 (**a**) and MTF2 (**b**) Tudor-PHD1-PHD2-EH cassettes with histone peptides. Data are representative of at least two independent experiments. **c**, Structural alignment of the PHF1-DNA-histone ternary

complex (in blue) with that of the MTF2 ternary complex (in magenta). The PHF1-bound H3K36me3 peptide is coloured in yellow, and K36me3 is shown in a space-filling representation. **d, e**, Structural details of the interactions between the H3K36me3 peptide and the PHF1 cassette (**d**) or the MTF2 cassette (**e**) in their ternary complexes.

winged-helix motif makes sequence-specific contacts with the target DNA through both the third  $\alpha$ -helix and the W1 loop<sup>22</sup> (Extended Data Fig. 3c–e).

PCL proteins show high sequence similarities within their EH regions (Extended Data Fig. 1a), indicating that other PCL members may also recognize CpG-containing DNAs. Indeed, both MTF2 and PHF19 Tudor-PHD1-PHD2-EH cassettes bind the 12-mer-CpG DNA, while mutating either of the first two lysine residues in their Ile-Lys-Lys-Lys-Lys motifs (Ile-Lys-Lys-Arg-Lys in PHF1) results in a complete loss of binding (Fig. 2e). Sequence alignments show that the CpG-recognizing Ile-Lys-Lys-(Arg/Lys)-Lys motif in the W1 loop is conserved in vertebrate PCL EH<sub>WH</sub> domains (less so in *Drosophila*), but is absent in other winged-helix motifs (Extended Data Fig. 1b), suggesting that the CpG-recognition mechanism by the winged-helix motif is unique to the PCL proteins.

In the crystal structure, PHF1 makes a sequence-specific interaction with a four-base segment of the bound DNA. To identify detailed CpG-containing motifs recognized by the PCL proteins, we used ITC and EMSA methods to measure the binding affinities of both the PHF1 and MTF2 PHD2-EH fragments for all 10 possible combinations of the NCpGN-containing DNA duplexes (N denotes any DNA base; Extended Data Fig. 2b, c and Extended Data Tables 2 and 3). Both PHF1 and MTF2 showed higher binding affinity for the (G/T)CpGG containing sequences. To validate the DNA motifs recognized by PCL proteins further, we performed unbiased protein binding microarray experiments using universal ‘all 10mer’ arrays<sup>23</sup>, which confirmed that PHF1 and MTF2 preferentially bind to DNAs containing the (T/G) CpGG motifs, with guanine residues slightly preferred as the flanking bases on each side of the motifs (Fig. 2f).

Both the PHF1 and MTF2 Tudor-PHD1-PHD2-EH cassettes favour binding to the H3K36me3 peptide over the H3K27me3 peptide (Fig. 3a, b), similar to the results from isolated Tudor domains<sup>4,6,7,11,15,16</sup>, suggesting that the presence of the other domains does not interfere with the histone-binding preference. In addition, we confirmed that the Tudor domains rather than the PHD1/2 fingers are responsible for the above recognition, as mutation of an aromatic-cage residue in the Tudor domain (Tyr47Ala for PHF1, Tyr62Ala for MTF2) led to a complete loss in binding affinity (Extended Data Table 2).

To clarify the relationship of DNA and histone binding activities further, we solved the crystal structures of the ternary complexes of both PHF1 and MTF2 Tudor-PHD1-PHD2-EH cassettes with bound 12-mer-CpG DNA bearing a 3' overhang thymine residue in the presence of the H3K36me3 peptide (Extended Data Table 1). The structures of both complexes superimpose well with each other except that their PHD1 domains display a small overall offset (Fig. 3c). The histone and DNA binding occur independently at the Tudor domain and the EH<sub>WH</sub> domain, respectively. Of note, the Lys36me3-engaging aromatic cage of PHF1 is composed of four aromatic residues (Fig. 3d), whereas in MTF2, the fourth aromatic residue is replaced by Ser86 (Fig. 3e). In addition, the PHF1-histone binding is further stabilized by sequence-specific interactions between Lys37 of H3 with Glu66 from the Tudor domain, and Arg40 of H3 with the residues located in the linker region between PHD1 and PHD2 (Fig. 3d). By contrast, MTF2 contacts only the backbone of the histone peptide (Fig. 3e). These differences may account for the relatively weaker binding affinity of MTF2 for the H3K36me3 peptide (Fig. 3b).

PCL proteins have been proposed to be involved in recruiting PRC2 to chromatin<sup>4,6,10,12,24</sup>. Analysis of publically available data<sup>10,12</sup> demonstrated that MTF2 and PHF19 colocalize with PRC2 at a subset of unmethylated CpG island-containing promoters in mouse embryonic stem (ES) cells (Fig. 4a). Their binding locations show enrichment of CpG-rich DNA motifs (Fig. 4b), supporting a potential role of EH<sub>WH</sub> for the recruitment of PRC2 to these target genes. To investigate this hypothesis in more detail, we focused on MTF2, which is the dominant PCL protein in mouse ES cells<sup>25</sup>. MTF2 is expressed in mouse ES cells in three distinct isoforms owing to alternative translational start sites<sup>24</sup> (Extended Data Fig. 4a, b). We obtained MTF2-knockout mouse ES cells by disrupting the *Mtf2* gene behind the third translational start site using CRISPR-Cas9 (Extended Data Fig. 4c–e). Consistent with a positive role of MTF2 for the function of PRC2, we observed in the knockout cells a reduced chromatin association of SUZ12 and de-repression of PRC2 target genes (Fig. 4c, Extended Data Fig. 4e, f and Extended Data Table 4). Rescue experiments using either wild-type MTF2 (isoform 2) or a CpG-binding deficient Lys339Ala-mutated MTF2 (Fig. 2e) demonstrated that the mutant has impaired chromatin binding ability (Fig. 4d). Consistently, the wild-type but not the mutant

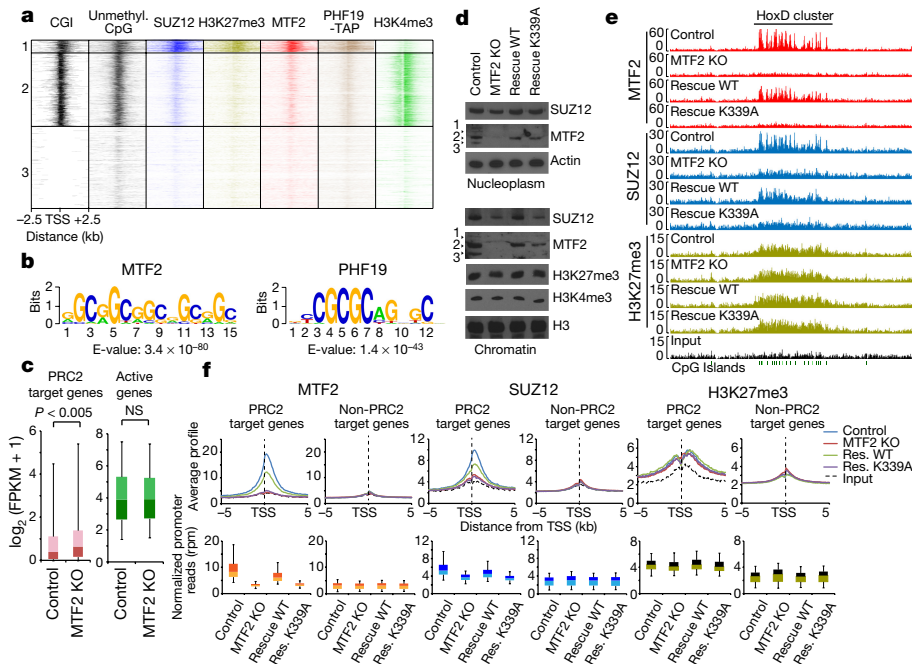


**Figure 4 | The MTF2 EH domain is essential for PRC2 recruitment in mouse ES cells.** **a**, Heat map of MTF2<sup>12</sup>, tandem affinity purification (TAP)-tagged PHF19<sup>10</sup>, unmethylated CpGs<sup>29</sup> and SUZ12<sup>10</sup> at three promoter groups: CpG island (CGI)-containing promoters enriched for SUZ12 (group 1,  $n = 2,008$ ), CGI-containing promoters with low SUZ12 (group 2,  $n = 11,743$ ) or promoters without CGI (group 3,  $n = 13,117$ ). **b**, Enriched DNA motifs at MTF2- and PHF19-bound locations. **c**, Gene expression (RNA-seq) of control and MTF2-knockout (KO) cells at PRC2 target genes and active non-PRC2 target genes (fragments per kilobase of transcript per million mapped reads (FPKM) > 1). The significance was estimated by one-way ANOVA with Tukey's post hoc test. NS, not significant. **d**, Western blotting of nucleoplasmic and chromatin fraction from mouse ES cells that express endogenous MTF2 (control), no MTF2

(MTF2 KO) or reintroduced wild-type (rescue WT) and Lys339Ala mutant (rescue K339A) MTF2 (isoform 2). Data are representative of two independent experiments. **e**, Genome browser view of the HoxD cluster for ChIP-seq data acquired from the four cell lines described. **f**, Promoter profiles of MTF2, SUZ12 and H3K27me3 at PRC2 target genes (group 1 as in **a**) or non-PRC2 target genes (groups 2 and 3) in the four investigated cell lines. Normalized ChIP-seq promoter reads are presented as whisker plots. ChIP-seq experiments were performed in three biological replicates, which were combined for the analysis (see also Extended Data Fig. 5a). The whisker-box plots represent the lower quartile, median and upper quartile of the data with 5% and 95% whiskers. Uncropped blots are shown in Supplementary Fig. 1.

MTF2 was able to partially rescue the gene expression levels and the chromatin association of SUZ12 (Fig. 4d and Extended Data Fig. 4g, h). To obtain a more comprehensive picture, we performed chromatin immunoprecipitation followed by sequencing (ChIP-seq) experiments for MTF2, SUZ12 and H3K27me3 in control, MTF2-knockout, and rescued cells (Extended Data Fig. 5a). Comparison of MTF2 ChIP-seq data in control and knockout cells confirmed that MTF2 is strongly enriched at PRC2 target genes, and only subtly bound to CpG islands at active genes (Extended Data Fig. 5b). The lost chromatin association of MTF2 and SUZ12 in MTF2-knockout cells could partially be restored when wild-type MTF2 but not the Lys339Ala mutant was re-expressed (Fig. 4e, f), demonstrating a crucial role of the EH<sub>WH</sub> domain for the chromatin binding of MTF2 and PRC2. By contrast, H3K27me3 was only mildly affected by the level of chromatin-bound MTF2 (Fig. 4e, f), which is similar to the previously observed minor consequences on H3K27me3 levels after MTF2 or PHF19 depletion *in vivo*<sup>9,10</sup> (Extended Data Fig. 5c). To address further the role of the MTF2 EH<sub>WH</sub> with respect to the function of PRC2, we purified human MTF2 containing PRC2 from HeLa-S cells (Extended Data Fig. 6a, b). EMSA experiments demonstrated that wild-type but not mutant MTF2-PRC2 can bind to the 12-mer-CpG DNA (Extended Data Fig. 6c), suggesting that other than the MTF2 EH<sub>WH</sub> domain, no other parts of MTF2-PRC2 can bind to CpG motifs. Consistently, the mutant MTF2-PRC2 possesses reduced methyltransferase activity on nucleosomes *in vitro* (Extended Data Fig. 6d). Together these data support a critical function of the MTF2 EH<sub>WH</sub> domain for the recruitment of PRC2 to chromatin.

Overall, the structural and biochemical analyses of both the PHF1 and the MTF2 N-terminal cassettes establish the PCL EH<sub>WH</sub> motifs as

a new family of unmethylated CpG-containing DNA binding motifs, comparable to the canonical CpG-recognizing CXXC domains identified 17 years ago<sup>26</sup>. Unexpectedly, despite the structural divergence, PHF1/MTF2 EH<sub>WH</sub> and CFP1 CXXC<sup>27</sup> use similar principles underlying CpG DNA recognition (Extended Data Fig. 3f–h). PRC2 and its associated PCL proteins are commonly located at CpG islands<sup>14</sup>. Our finding that PCL proteins specifically recognize unmethylated CpG motifs through their EH<sub>WH</sub> domains provides a direct link between CpG islands and PRC2 recruitment. Given that Polycomb-related gene regulation has been implicated in carcinogenesis<sup>1</sup>, our finding may provide a new target for therapeutic intervention.

**Online Content** Methods, along with any additional Extended Data display items and Source Data, are available in the online version of the paper; references unique to these sections appear only in the online paper.

Received 23 August 2016; accepted 25 July 2017.

Published online 6 September 2017.

- Comet, I., Riising, E. M., Leblanc, B. & Helin, K. Maintaining cell identity: PRC2-mediated regulation of transcription and cancer. *Nat. Rev. Cancer* **16**, 803–810 (2016).
- Margueron, R. & Reinberg, D. The Polycomb complex PRC2 and its mark in life. *Nature* **469**, 343–349 (2011).
- Hauri, S. *et al.* A high-density map for navigating the human Polycomb complexome. *Cell Reports* **17**, 583–595 (2016).
- Ballaré, C. *et al.* Phf19 links methylated Lys36 of histone H3 to regulation of Polycomb activity. *Nat. Struct. Mol. Biol.* **19**, 1257–1265 (2012).
- Boulay, G., Rosnoblet, C., Guérardel, C., Angrand, P. O. & Leprince, D. Functional characterization of human Polycomb-like 3 isoforms identifies them as components of distinct EZH2 protein complexes. *Biochem. J.* **434**, 333–342 (2011).
- Brien, G. L. *et al.* Polycomb PHF19 binds H3K36me3 and recruits PRC2 and demethylase NO66 to embryonic stem cell genes during differentiation. *Nat. Struct. Mol. Biol.* **19**, 1273–1281 (2012).

7. Cai, L. *et al.* An H3K36 methylation-engaging Tudor motif of polycomb-like proteins mediates PRC2 complex targeting. *Mol. Cell* **49**, 571–582 (2013).
8. Cao, R. *et al.* Role of hPHF1 in H3K27 methylation and Hox gene silencing. *Mol. Cell. Biol.* **28**, 1862–1872 (2008).
9. Casanova, M. *et al.* Polycomblike 2 facilitates the recruitment of PRC2 Polycomb group complexes to the inactive X chromosome and to target loci in embryonic stem cells. *Development* **138**, 1471–1482 (2011).
10. Hunkapiller, J. *et al.* Polycomb-like 3 promotes polycomb repressive complex 2 binding to CpG islands and embryonic stem cell self-renewal. *PLoS Genet.* **8**, e1002576 (2012).
11. Musselman, C. A. *et al.* Molecular basis for H3K36me3 recognition by the Tudor domain of PHF1. *Nat. Struct. Mol. Biol.* **19**, 1266–1272 (2012).
12. Walker, E. *et al.* Polycomb-like 2 associates with PRC2 and regulates transcriptional networks during mouse embryonic stem cell self-renewal and differentiation. *Cell Stem Cell* **6**, 153–166 (2010).
13. Sarma, K., Margueron, R., Ivanov, A., Pirrotta, V. & Reinberg, D. Ezh2 requires PHF1 to efficiently catalyze H3 lysine 27 trimethylation *in vivo*. *Mol. Cell. Biol.* **28**, 2718–2731 (2008).
14. Ku, M. *et al.* Genomewide analysis of PRC1 and PRC2 occupancy identifies two classes of bivalent domains. *PLoS Genet.* **4**, e1000242 (2008).
15. Kycia, I. *et al.* The Tudor domain of the PHD finger protein 1 is a dual reader of lysine trimethylation at lysine 36 of histone H3 and lysine 27 of histone variant H3t. *J. Mol. Biol.* **426**, 1651–1660 (2014).
16. Qin, S. *et al.* Tudor domains of the PRC2 components PHF1 and PHF19 selectively bind to histone H3K36me3. *Biochem. Biophys. Res. Commun.* **430**, 547–553 (2013).
17. Holm, L. & Rosenström, P. Dali server: conservation mapping in 3D. *Nucleic Acids Res.* **38**, W545–9 (2010).
18. Callebaut, I. & Moron, J. P. The PWAPA cassette: Intimate association of a PHD-like finger and a winged-helix domain in proteins included in histone-modifying complexes. *Biochimie* **94**, 2006–2012 (2012).
19. Clark, K. L., Halay, E. D., Lai, E. & Burley, S. K. Co-crystal structure of the HNF-3/ fork head DNA-recognition motif resembles histone H5. *Nature* **364**, 412–420 (1993).
20. Biggs, W. H., III, Cavenee, W. K. & Arden, K. C. Identification and characterization of members of the FKHR (FOX O) subclass of winged-helix transcription factors in the mouse. *Mamm. Genome* **12**, 416–425 (2001).
21. Jones, P. A. Functions of DNA methylation: islands, start sites, gene bodies and beyond. *Nat. Rev. Genet.* **13**, 484–492 (2012).
22. Gajiwala, K. S. *et al.* Structure of the winged-helix protein hRFX1 reveals a new mode of DNA binding. *Nature* **403**, 916–921 (2000).
23. Berger, M. F. *et al.* Compact, universal DNA microarrays to comprehensively determine transcription-factor binding site specificities. *Nat. Biotechnol.* **24**, 1429–1435 (2006).
24. Li, X. *et al.* Mammalian polycomb-like Pcl2/Mtf2 is a novel regulatory component of PRC2 that can differentially modulate polycomb activity both at the Hox gene cluster and at Cdkn2a genes. *Mol. Cell. Biol.* **31**, 351–364 (2011).
25. Kloet, S. L. *et al.* The dynamic interactome and genomic targets of Polycomb complexes during stem-cell differentiation. *Nat. Struct. Mol. Biol.* **23**, 682–690 (2016).
26. Voo, K. S., Carlone, D. L., Jacobsen, B. M., Flodin, A. & Skalnik, D. G. Cloning of a mammalian transcriptional activator that binds unmethylated CpG motifs and shares a CXXC domain with DNA methyltransferase, human trithorax, and methyl-CpG binding domain protein 1. *Mol. Cell. Biol.* **20**, 2108–2121 (2000).
27. Xu, C., Bian, C., Lam, R., Dong, A. & Min, J. The structural basis for selective binding of non-methylated CpG islands by the CFP1 CXXC domain. *Nat. Commun.* **2**, 227 (2011).
28. Berger, M. F. & Bulyk, M. L. Universal protein-binding microarrays for the comprehensive characterization of the DNA-binding specificities of transcription factors. *Nat. Protocols* **4**, 393–411 (2009).
29. Xiao, S. *et al.* Comparative epigenomic annotation of regulatory DNA. *Cell* **149**, 1381–1392 (2012).

**Supplementary Information** is available in the online version of the paper.

**Acknowledgements** We thank the staff from the BL17U1, BL18U1 and BL19U1 beamlines of National Facility for Protein Science in Shanghai (NFPS) at Shanghai Synchrotron Radiation Facility (SSRF) in China for assistance during data collection, and C. Yun for help in data collection in the United States. We thank G. Jiang for help with ITC studies. We thank A. Jambhekar for critical reading of the manuscript. This work was supported by the National Natural Science Foundation of China (31370719 and 31570729), Beijing Natural Science Foundation (5152015) and the Fundamental Research Funds for the Central Universities (2014KJCA09 and 2017EYT19) to Z.W. Early research on PCL protein expression undertaken by Z.W. in the laboratory of D.J.P. was supported by the Leukemia and Lymphoma Society and by the Memorial Sloan-Kettering Cancer Center Core Grant (P30 CA008748). Research on PCL proteins was supported by the German Research Foundation (DFG, LI 2057/1-1) to R.L., NIH/NHGRI R01 grant HG003985 to M.L.B., and the National Cancer Institute (R01 CA118487) and funds from Boston Children's Hospital to Y.S. Y.S. is an American Cancer Society Research Professor.

**Author Contributions** H.L. performed the protein expression, purification and the crystallographic studies. R.L. performed experiments in mouse ES cells, genome-wide analyses and MTF2 complex experiments. J.J. did the ITC and EMSA assays. J.V.K. performed protein binding microarray experiments. W.T., P.D., W.Z. and Q.H. assisted in cloning and protein purification. M.L.B. supervised the protein binding microarray research. All authors analysed the data. Z.W. initialized the project, determined the crystal structures, designed the experiments with R.L. and Y.S., and wrote the paper with the help of R.L., D.J.P., J.V.K., M.L.B. and Y.S.

**Author Information** Reprints and permissions information is available at [www.nature.com/reprints](http://www.nature.com/reprints). The authors declare competing financial interests: details are available in the online version of the paper. Readers are welcome to comment on the online version of the paper. Publisher's note: Springer Nature remains neutral with regard to jurisdictional claims in published maps and institutional affiliations. Correspondence and requests for materials should be addressed to Z.W. ([wangz@bnu.edu.cn](mailto:wangz@bnu.edu.cn)).

**Reviewer Information** *Nature* thanks L. Chen, L. Di Croce and R. Klose for their contribution to the peer review of this work.

## METHODS

No statistical methods were used to predetermine sample size. The experiments were not randomized and the investigators were not blinded to allocation during experiments and outcome assessment.

X-ray statistics are listed in Extended Data Table 1. ITC binding parameters are listed in Extended Data Table 2. DNA names and sequences are listed in Extended Data Table 3. Real-time PCR primers are presented in Extended Data Table 4.

**Protein expression and purification.** Constructs containing the PHF1 or MTF2 cassettes were made by inserting the corresponding cassettes into a hexahistidine-SUMO-tagged pRSFDuet-1 vector. The protein was expressed in *Escherichia coli* Rosetta (DE3) cells at 37°C until the OD<sub>600 nm</sub> reached around 1.0, then the cells were cooled at 20°C for around 1 h before 0.2 mM IPTG and 0.1 mM ZnCl<sub>2</sub> were added to induce expression overnight. Cells were collected by centrifugation at 4,500g for 20 min. Cell pellets were re-suspended with the initial buffer containing 20 mM Tris, pH 7.0, 500 mM NaCl, 20 mM imidazole and sonicated for around 5 min. The soluble fraction of the cells was fractionated by centrifugation of the cell lysate at 25,000g for 1 h. Histidine-SUMO-tagged target protein was isolated through a nickel-charged HiTrap Chelating FF column from GE Healthcare. The histidine-SUMO tag was then cleaved by incubating with histidine-tagged ULP1 protease and dialysed with the initial buffer at 4°C. The dialysed solution was then reloaded onto a nickel-charged chelating column to remove both the histidine-tagged SUMO and ULP1. The flow through was diluted twofold with 20 mM Tris, pH 7.0, 2 mM DTT, to yield a solution with half the initial salt concentration (250 mM NaCl), which was then loaded directly onto a heparin column to remove bound DNA. Target protein was separated by increasing the salt concentration of the low-salt buffer (20 mM Tris, pH 7.0, 250 mM NaCl, 2 mM DTT) from 250 mM to 1 M NaCl through a linear gradient. The target protein was further purified by a hילוoad 200 16/600 gel-filtration column equilibrated with the low-salt buffer, through which the resulting product was eluted as a monomer with high purity. Purified proteins were concentrated to around 20 mg ml<sup>-1</sup> and stored in a -80°C freezer.

PHF19 (31–377) was not stable in buffers with salt concentration lower than 500 mM NaCl. To enhance its stability for the EMSA analysis, the PHF19 (31–377) fragment was cloned into a revised pRSFDuet-1 vector bearing a hexahistidine-MBP tag at the N terminus and a glutathione *S*-transferase (GST) tag at the C terminus. The expression and purification procedure is similar as that of PHF1 and MTF2, except that both the histidine-MBP tag and the GST tag were not removed.

**Crystallization and structure resolution.** Crystallization was carried out using the hanging-drop, vapour-diffusion method by mixing equal volume of protein and well solution. Crystals of both free forms of human PHF1 (26–340) were grown by mixing 1 µl protein at the concentration of 15 mg ml<sup>-1</sup> with 1 µl crystallization buffer containing 0.1 M Tris, pH 8.0, 10% PEG 3,350, 22% ethylene glycerol at 4°C. The crystals were picked and flash frozen directly in liquid nitrogen.

The binary complex of the human PHF1 (26–360) and DNA was prepared by mixing protein with the palindromic 12-mer-CpG DNA duplex bearing a 3'-overhang thymine (5'-GGGCGGCCGCCCT-3') at the molar ratio of 2:1.1. Crystals of the complex were grown under the condition of 0.1 M Tris, pH 8.5, 25% PEG 3,350, 0.2 M Li<sub>2</sub>SO<sub>4</sub>, 10 mM MgCl<sub>2</sub> at 4°C. Crystals were flash frozen in the crystallization buffer containing 12% 2,3-butanediol as the cryoprotectant.

The ternary complex of the mouse PHF1 (26–360)/DNA/H3(29–41)K36me3 was prepared by mixing PHF1, DNA and the peptide at the molar ratio of 2:1.1:1.5. Complex crystals were grown at 20°C in the crystallization buffer of 50 mM Bis-Tris, pH 6.5, 50 mM ammonium sulfate, 30% pentaerythritol ethoxylate (15/4 EO/OH), which was also used as the cryoprotectant.

The ternary complex of the human MTF2 (42–358)-DNA-H3(33–40)K36me3 was prepared by mixing MTF2, DNA and the histone peptide at the molar ratio of 2:1.1:1.5. Crystals of the complex were grown at 20°C in the crystallization buffer containing 0.1 M MES monohydrate, pH 6.5, 0.2 M ammonium sulfate, 25% PEG monomethyl ether 5,000, 10% glycerol. Crystallization buffer containing 20% glycerol was used as the cryoprotectant.

Datasets for the free form human PHF1 crystals were collected at Argonne National Laboratory APS 19ID beamline in the United States at the wavelength of 0.97918 Å. The datasets were processed using the program HKL2000. Structure determination was carried out by PHENIX<sup>30</sup> through the SAD method using zinc anomalous signals. The initial partial model was auto-built by the ARP/wARP<sup>31</sup>, then manually rebuilt by Coot<sup>32</sup>, and further refined by PHENIX. There is one PHF1 molecule in one crystallographic asymmetric unit.

Datasets for the human PHF1/DNA binary complex crystals were collected at the Shanghai Synchrotron Radiation Facility (SSRF) beamline BL18U1 in China at the wavelength of 0.97791 Å. The structure of the binary complex was solved by molecular replacement method by PHENIX using the free form PHF1 (26–340)

structure as the model. The structure of the binary complex was built and refined by the PHENIX program. There are three PHF1 molecules in one asymmetric unit, with one remaining in the free form, while the other two form a complex with a DNA duplex.

Datasets for the crystals of the mouse PHF1-DNA-histone ternary complex were collected at SSRF beamline BL19U1. The structure was solved by molecular replacement method using the free form PHF1 structure as the model. Model building and structure refinement are similar to that of the PHF1 binary complex structure.

Datasets for the human MTF2-DNA-histone ternary complex crystals were collected at SSRF beamline BL19U1 at the wavelength of 0.97853 Å. The structure of the ternary complex was solved by molecular replacement method using the free form PHF1 structure as the model. Model building and refinement were similar to that of the PHF1 binary complex structure.

**EMSA.** Double-stranded DNA (75 pmol) was mixed with increasing amounts of recombinant PCL proteins in the buffer containing 20 mM Tris, pH 7.0, 200 mM NaCl and 2 mM DTT, and incubated at 4°C for 20 min. The mixture was then loaded on a 1.2% agarose gel in the TAE buffer for electrophoresis and detected by ethidium bromide staining. Constructs containing PHF1 (26–360) and MTF2 (42–378) were used for the assay. To enhance the solubility of PHF19, a construct containing PHF19 (31–377) plus an N-terminal hexahistidine-MBP tag and a C-terminal GST tag was used for the assay. All EMSA experiments were repeated at least three times.

**ITC measurement.** Calorimetric experiments were carried out at 10°C with a MicroCal iTC200 instrument. To obtain better results, purified wild-type or mutant proteins or DNA duplexes were dialysed overnight at 4°C in the titration buffer containing 20 mM Tris, pH 7.0, 150 mM NaCl and 2 mM β-mercaptoethanol. Histone peptides were prepared by dissolving small aliquots of lyophilized peptides with the same buffer just before use. Titration was performed by injecting histone peptides or DNA fragments into protein samples. Calorimetric titration data were fitted with the Origin software under the algorithm of one binding-site model. All ITC measurements have been repeated at least twice.

**Cell culture, cellular fractionation, RNA-seq, ChIP and antibodies.** Embryonic day (E) 14 mouse ES cells (E14TG2a) were obtained from ATCC and cultured in DMEM, 15% FCS, 1 × L-glutamine (Invitrogen), 1 × non-essential amino acids (Invitrogen), 1 × sodium pyruvate, 1 × penicillin/streptomycin (Invitrogen), 0.15% β-mercaptoethanol and 100 U ml<sup>-1</sup> of LIF (Millipore) on gelatin-coated plates. The cells were tested for mycoplasma contamination. Stable cell lines were obtained via infection with lentiviral vectors harbouring the appropriate construct and selected via puromycin or blasticidin. MTF2-knockouts experiments were performed using LentiCRISPRv2<sup>33</sup> with the following guide RNAs targets: (1: 5'-ATCACACTCGAGTCAATATG-3'; 2: 5'-AGGGGTGGTGCGCTTAAGAA-3'; 3: 5'-ACTGTAAACGGTAGACGTTG-3'; 4: 5'-AGAAGAAGAAGCATTTGTTT-3'). The gRNA target 4 was used to obtain MTF2-knockout cells. Single-cell clones were gained by limited dilution and validated by sequencing and western blotting. Rescue experiments were performed with lentiviral vectors expressing untagged mouse MTF2 (isoforms 2). The PAM sequence was synonymously mutated in rescue constructs.

Cellular fractionations were performed using the Subcellular Protein Fractionation Kit for Cultured Cells (Thermo Scientific, 78840) according to manufacturer's instructions, followed by western blotting. ChIP experiments were performed by cross-linking ChIP as described<sup>34</sup>. In short, 100 million cells were crosslinked with 1% formaldehyde for 10 min. Subsequently, the cells were treated first with lysis buffer 1 (50 mM Tris, pH 8.0, 2 mM EGTA, 0.1% NP-40, 10% glycerol) for 10 min, homogenized and centrifuged. The obtained pellet was incubated with lysis buffer 2 (50 mM Tris, pH 8.0, 2 mM EGTA, 1% SDS) for 10 min and sonicated with a Biorupter to gain DNA fragments of 200–500 base pairs. After centrifugation, the supernatant was diluted in dilution buffer (50 mM Tris, pH 8.0, 5 mM EGTA, 200 mM NaCl, 0.5% NP-40) and pre-cleared for 1 h using a protein A/G bead mix. Subsequently, 10–20 µg of antibody was added and the solution was incubated for 12 h at 4°C. The antibodies were bound using a protein A/G bead mix for 1 h. The beads were washed twice with NaCl buffer (20 mM Tris, pH 8.0, 500 mM NaCl, 2 mM EGTA) and twice with LiCl buffer (200 mM Tris, pH 8.0, 500 mM LiCl, 2 mM EGTA, 0.1% SDS, 1% NP-40). The precipitated DNA was eluted, de-crosslinked and purified by phenol-chloroform extraction. The obtained DNA was analysed via qPCR or next generation sequencing. Sequencing libraries were prepared using the NEBNext Ultra DNA Library Prep Kit for Illumina (NEB, E7370) with 10–20 ng DNA. For RNA-seq, whole RNA was prepared using Trizol and purified using Magnetic beads mRNA Isolation Kit (BioLabs, S1505). After mRNA fragmentation by heating the sample for 6 min at 95°C, the mRNA was reverse transcribed using SuperScript III (Invitrogen, 18080-044), followed by Second Strand Synthesis (Invitrogen, 10812-014).

RNA-seq libraries were constructed of 10–50 ng DNA using NEBNext DNA Library Prep Reagent Set (NEB, E6000). RNA-seq and ChIP-seq libraries were analysed using the Illumina HiSeq 2500 System, and performed in three biological replicates.

The following antibodies were used: SUZ12 (Santa Cruz, sc-46264; for western), SUZ12 (D39F6, Cell Signaling; for ChIP), actin (abcam, ab3280), histone H3 (abcam, ab1791), H3K27me3 (Millipore, 07-449), H3K4me3 (Millipore, 04-745) and MTF2 (Proteintech, 16208-1-AP).

**EMSA and HMTase reaction with human MTF2 complexes.** HeLa-S cells were infected with Lentiviral constructs expressing human full-length Flag- and haemagglutinin (HA)-tagged MTF2 or Flag-HA-MTF2(Lys339Ala). MTF2 complexes and empty vector mock control were obtained in parallel from 5l HeLa-S cultures via single step purification using anti-Flag (M2) conjugated agarose beads (Sigma, A2220). Bound proteins were washed three times with TAP-buffer (50 mM Tris, pH 7.9, 100 mM KCl, 5 mM MgCl<sub>2</sub>, 0.2 mM EDTA, 10% glycerol, 0.2 mM PMSF, 1 mM DTT, 0.1% NP-40) and subsequently eluted with 50 µl TAP-buffer containing 1 µg ml<sup>-1</sup> Flag peptide. 1 µl of the eluate was analysed by Silver staining. EMSA was performed with equal volumes (0.5, 1, 2 and 3 µl) of the eluates using the 12-mer-CpG sequence. For the HMTase assay, mononucleosomes were incubated with 15 µl of the eluates for 2 h at 25 °C using the following reaction buffer: 10 mM HEPES, pH 7.4, 50 mM NaCl, 10 µM ZnCl<sub>2</sub>, 0.5 mM DTT, 2.5 mM MgCl<sub>2</sub>, 2 mM ATP, 5% glycerol and 80 µM SAM<sup>35</sup>. The reaction products were analysed by western blotting.

**Bioinformatics analyses.** RNA-seq data were analysed using TopHat and Cuffdiff<sup>36</sup>. ChIP-seq data were aligned to mouse genome mm9 using Bowtie 1.0<sup>37</sup> with  $n = 1$  and  $m = 3$  as parameter. Normalized Bigwig files were obtained using DeepTools<sup>38</sup>. Bioinformatics analyses were performed via the Cistrome platform<sup>39</sup> or Bioconductor<sup>40</sup>. Promoter reads were counted from -2000 to +2000 relative to the transcription start site and normalized to reads per million (rpm). The following public datasets were used: SUZ12 (GSM700554, GSM700553), PHF19 (GSM700556, GSM700555)<sup>10</sup>, MTF2 (GSM415050)<sup>12</sup>, MRE-Seq (GSM881347)<sup>29</sup> and H3K4me3 (GSM2027596)<sup>34</sup>. CpG island and promoter definitions were downloaded from the UCSC browser. Enriched motifs were identified by MEME-ChIP<sup>41</sup>.

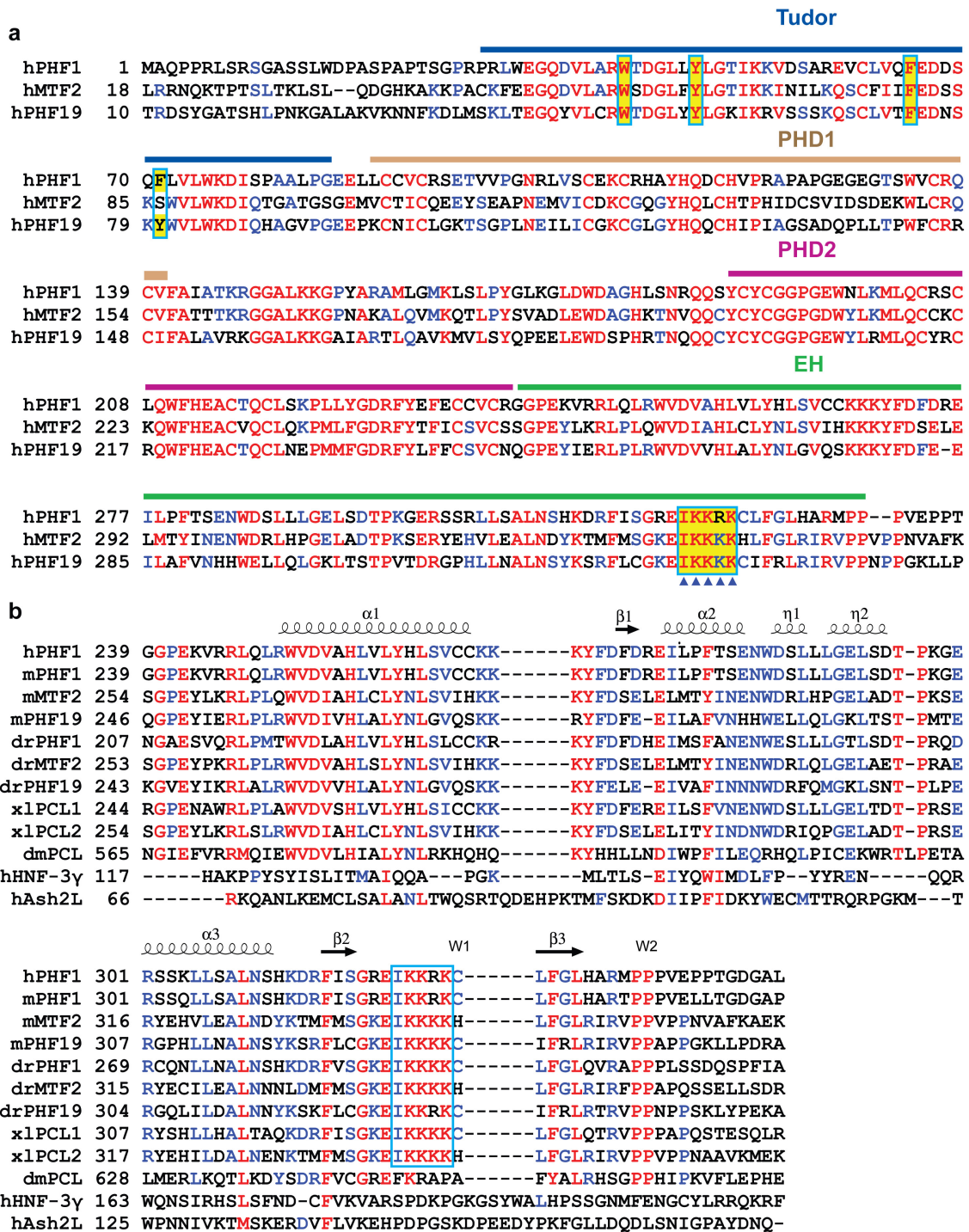
**Protein binding microarray experiments and analysis.** GST-fusion proteins for human PHF1 (165–360) and MTF2 (180–369) were expressed in BL21 (DE3) cells and affinity purified using glutathione beads (Amersham). Subsequently, custom-designed 'all-10mer' universal oligonucleotide arrays in 8 × 60K GSE array format (Agilent Technologies; AMADID 030236) were double-stranded and duplicate protein binding microarray experiments were performed essentially as described<sup>23,28</sup>. MTF2 was assayed at a final concentration of either 500 nM or

900 nM, while PHF1 was assayed at a final concentration of 900 nM, in binding reactions containing 50 µM zinc acetate, on either a fresh slide or a slide that had been stripped exactly once. Scans were acquired using a GenePix 4400A (Molecular Devices) microarray scanner. Microarray data quantification, normalization, and motif derivation were performed essentially as described previously using the Universal PBM Analysis Suite and the Seed-and-Wobble motif-derivation algorithm<sup>23,28</sup>.

**Statistical analysis.** For statistical comparisons of two groups, one-way ANOVA followed by Tukey's post hoc test was used.

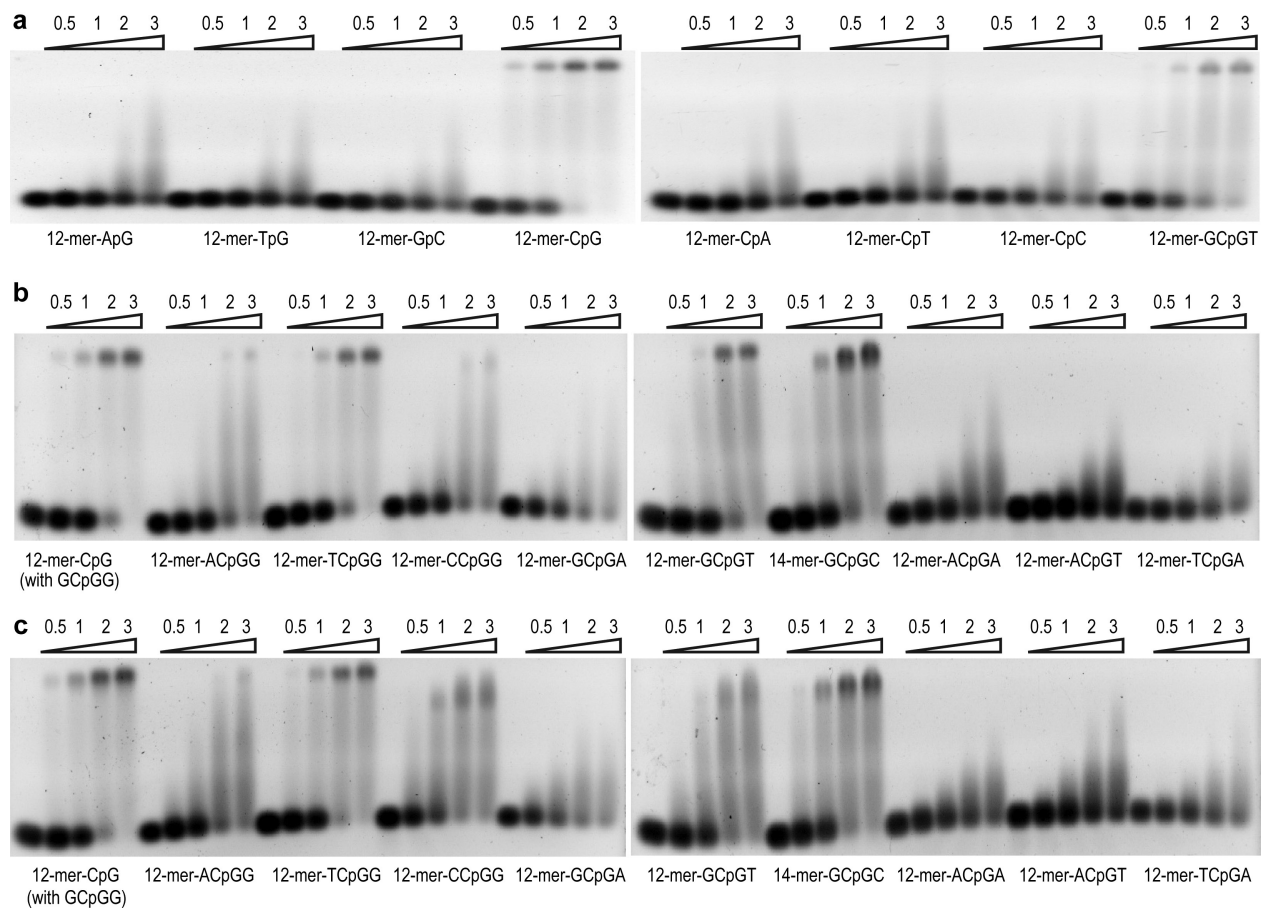
**Data availability.** Atomic coordinates and structure factors for the apo-form PHF1 in two crystal forms, the binary complex of PHF1–DNA, and the ternary complexes of PHF1–DNA–histone and MTF2–DNA–histone have been deposited in the Protein Data Bank (PDB) under the accession codes 5XFN, 5XFO, 5XFP, 5XFQ and 5XFR, respectively. ChIP-seq and RNA-seq data are available at the Gene Expression Omnibus (GEO) repository under accession GSE97805. PBM data are available in the UniPROBE database (UniPROBE accession KUR17A).

30. Adams, P. D. *et al.* PHENIX: a comprehensive Python-based system for macromolecular structure solution. *Acta Crystallogr. D* **66**, 213–221 (2010).
31. Langer, G., Cohen, S. X., Lamzin, V. S. & Perrakis, A. Automated macromolecular model building for X-ray crystallography using ARP/wARP version 7. *Nat. Protocols* **3**, 1171–1179 (2008).
32. Emsley, P., Lohkamp, B., Scott, W. G. & Cowtan, K. Features and development of Coot. *Acta Crystallogr. D* **66**, 486–501 (2010).
33. Sanjana, N. E., Shalem, O. & Zhang, F. Improved vectors and genome-wide libraries for CRISPR screening. *Nat. Methods* **11**, 783–784 (2014).
34. Liefke, R., Karwacki-Neisius, V. & Shi, Y. EPOP interacts with Elongin BC and USP7 to modulate the chromatin landscape. *Mol. Cell* **64**, 659–672 (2016).
35. Kalb, R. *et al.* Histone H2A monoubiquitination promotes histone H3 methylation in Polycomb repression. *Nat. Struct. Mol. Biol.* **21**, 569–571 (2014).
36. Trapnell, C. *et al.* Differential gene and transcript expression analysis of RNA-seq experiments with TopHat and Cufflinks. *Nat. Protocols* **7**, 562–578 (2012).
37. Langmead, B., Trapnell, C., Pop, M. & Salzberg, S. L. Ultrafast and memory-efficient alignment of short DNA sequences to the human genome. *Genome Biol.* **10**, R25 (2009).
38. Ramírez, F., Dündar, F., Diehl, S., Grüning, B. A. & Manke, T. deepTools: a flexible platform for exploring deep-sequencing data. *Nucleic Acids Res.* **42**, W187–W191 (2014).
39. Liu, T. *et al.* Cistrome: an integrative platform for transcriptional regulation studies. *Genome Biol.* **12**, R83 (2011).
40. Gentleman, R. C. *et al.* Bioconductor: open software development for computational biology and bioinformatics. *Genome Biol.* **5**, R80 (2004).
41. Bailey, T. L. *et al.* MEME SUITE: tools for motif discovery and searching. *Nucleic Acids Res.* **37**, W202–W208 (2009).



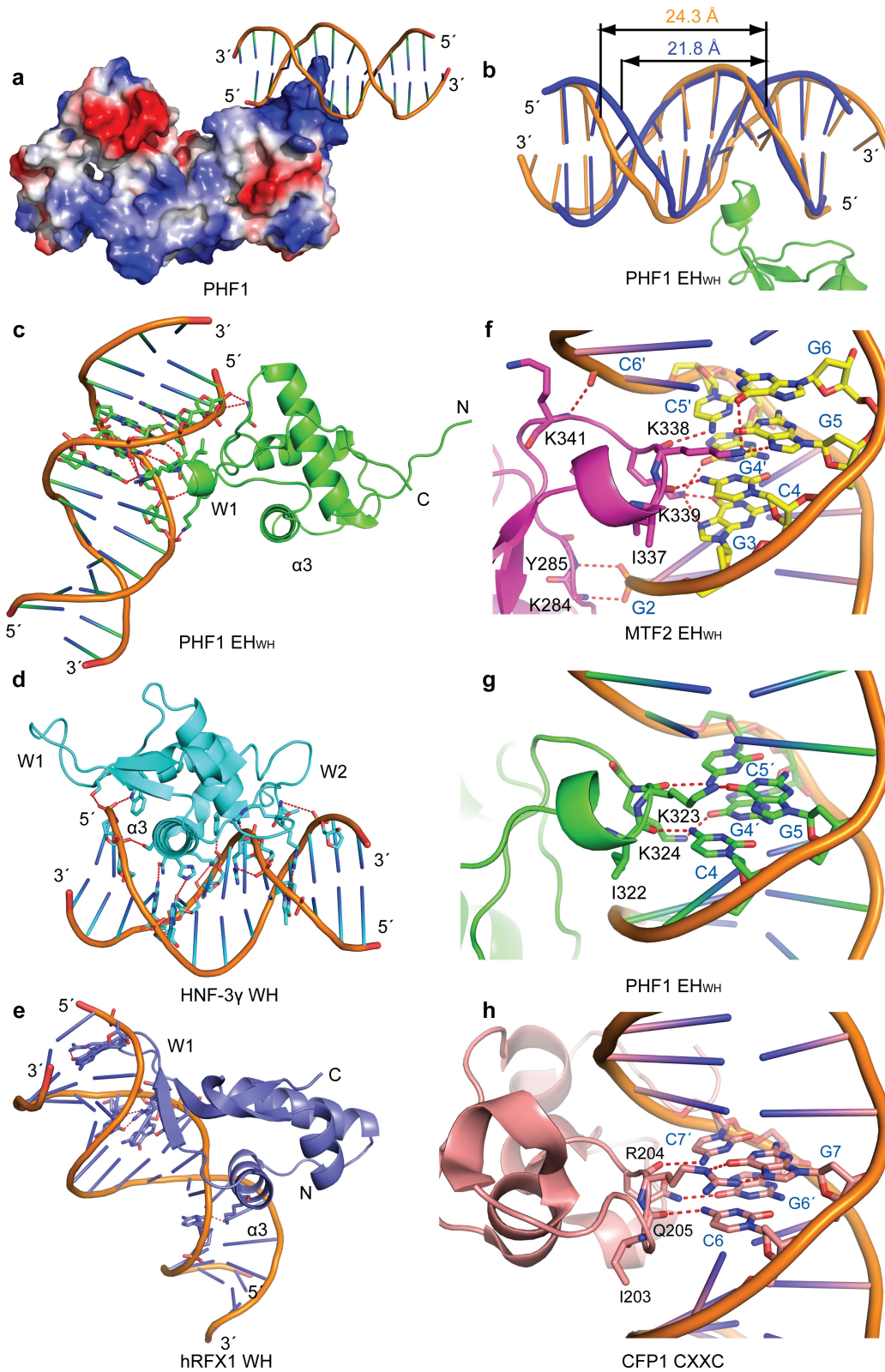
Extended Data Figure 1 | Sequence alignment of human PCL proteins, or the EH/WH regions from various species. a, Sequence alignment of the N-terminal domains of human PCL proteins. Residues with high similarity are coloured in red. Key residues mentioned in the text are highlighted yellow and indicated with blue triangles at the bottom.

b, Sequence alignment of the EH domains from various species of PCL proteins and two typical winged-helix motifs. Conserved IKK(K/R)K motifs within the W1 loop of various PCL proteins are indicated in a blue box. Species abbreviations: h, *Homo sapiens*; m, *Mus musculus*; dr, *Danio rerio*; xl, *Xenopus laevis*; dm, *Drosophila melanogaster*.



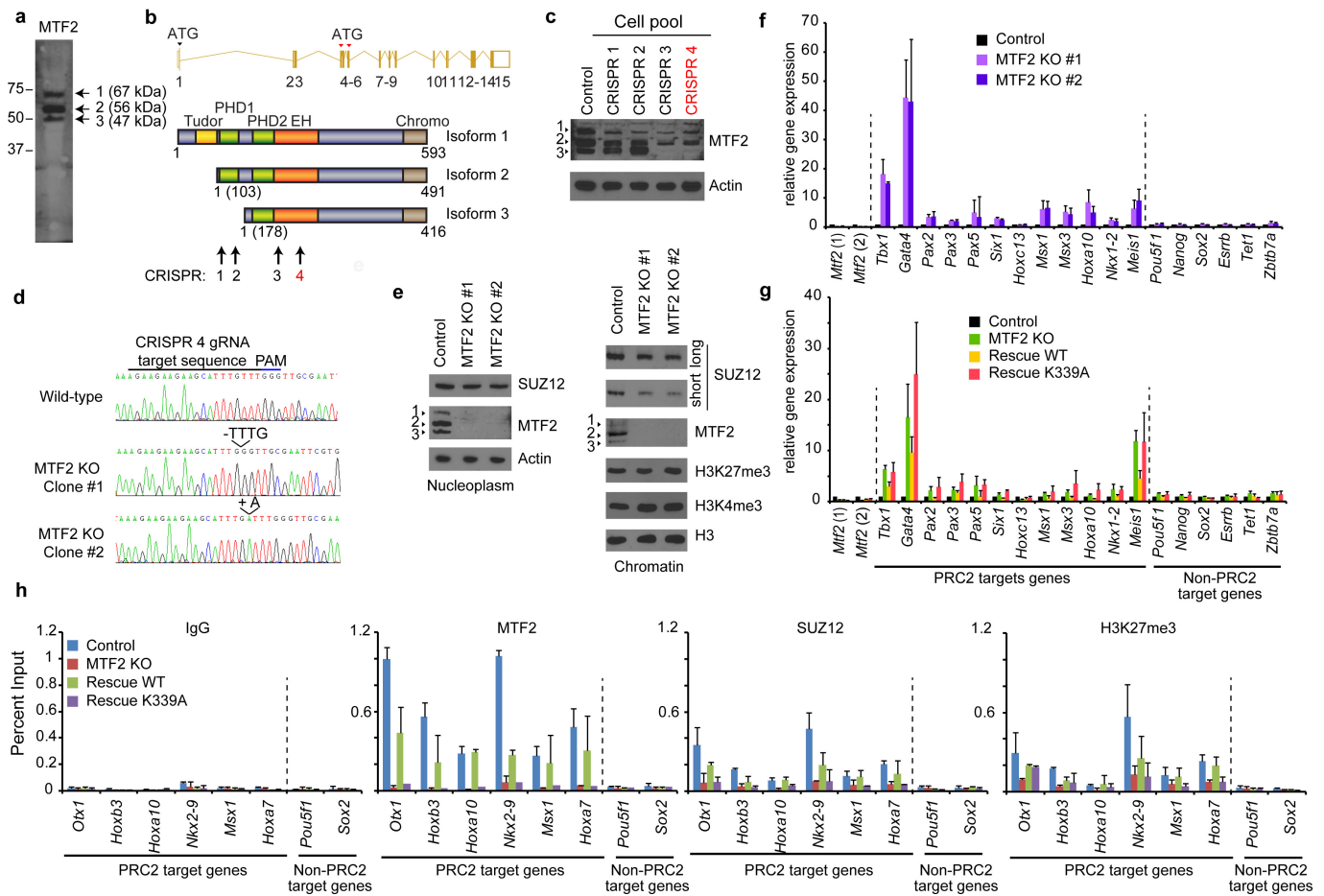
**Extended Data Figure 2 | Binding analysis of PCL proteins with different CpG-motif substitutions or with CpG-containing DNAs varying in their flanking sequences.** **a**, EMSA results of the PHF1(26–360) fragment with different DNA duplexes bearing base substitutions in the CpG motif. **b**, **c**, EMSA results of PHF1(165–360) (**b**)

or MTF2(180–378) (**c**) with various NCpGN-containing DNA motifs; N denotes any DNA base. The protein-to-DNA molar ratio is shown at the top. Data are representative of at least three independent experiments. Uncropped gels are shown in Supplementary Fig. 1.



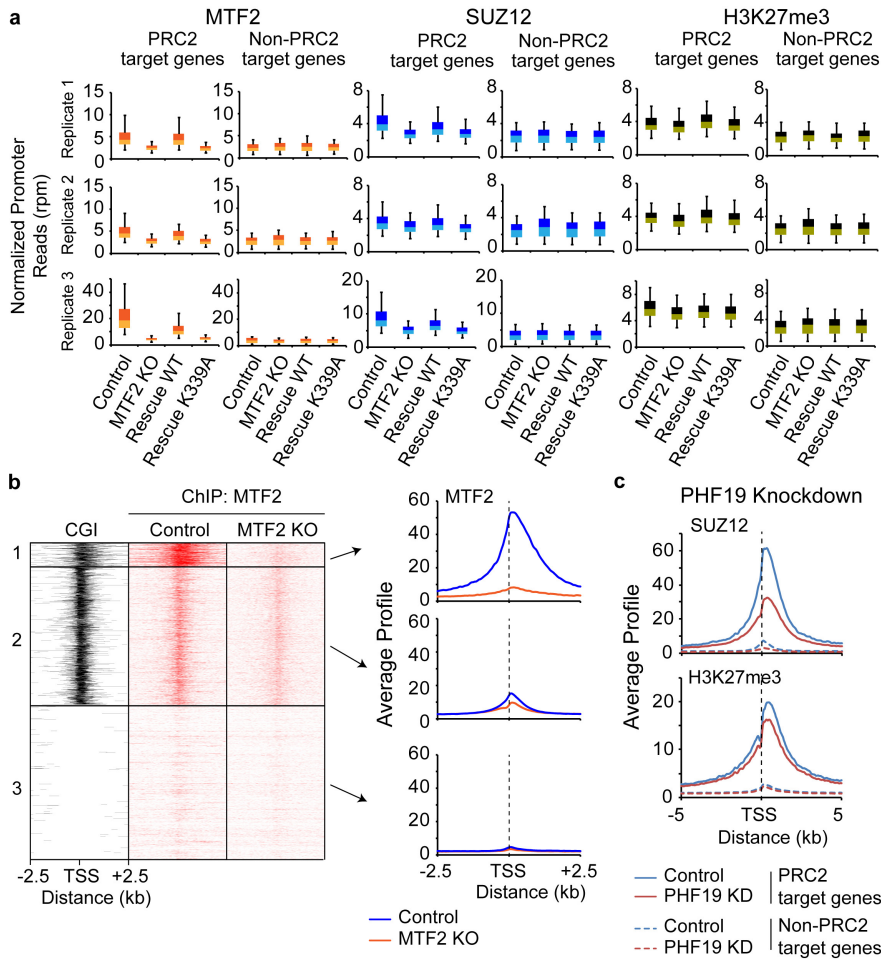
**Extended Data Figure 3 | Comparisons of DNA-bound PHF1 or MTF2 EH domains with two DNA-bound winged-helix motifs and a CXXC domain.** **a**, Electrostatic surface of the PHF1 cassette, with basic regions shown in blue and acidic regions in red. Bound DNA is shown in a cartoon representation. **b**, Superimposition of the PHF1-bound DNA (coloured in orange) with a canonical B-form DNA (coloured in blue; PDB code 1HQ7). **c–e**, Comparison of the DNA-recognizing details of the PHF1 EH domain (**c**) with the winged-helix motifs of HNF-3 $\gamma$  (**d**; PDB code 1VTN)

and hRFX1 (**e**; PDB code 1DP7) when all three domains were structurally aligned. **f–h**, Comparison of the CpG-recognition details of the MTF2 EH domain (**f**) and the PHF1 EH domain (**g**) with that of the CFP1 CXXC (**h**; PDB code 3QMC). Of note, both cytosine residues of the CpG duplex form hydrogen bonds with the main-chain carbonyl oxygens, while both guanines of the CpG duplex were also recognized by forming hydrogen bonds with the side chains.



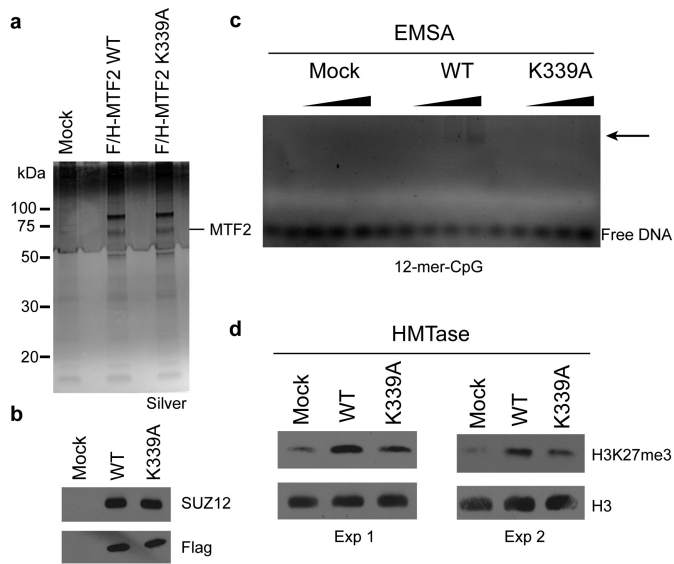
**Extended Data Figure 4 | Creation of MTF2-knockout mouse ES cells and qPCR experiments.** **a**, Representative western blot of endogenous MTF2 in mouse ES cells. Three distinct isoforms are indicated. **b**, Schematic overview of the three MTF2 isoforms and their corresponding translational start sites. Positions of four test CRISPR gRNA targets are shown. **c**, Western blot of mouse ES cells expressing a control of CRISPR construct or CRISPR constructs targeting the *Mtf2* gene as depicted in **b**. CRISPR 4 (in red) was used to obtain single cell clones. **d**, Sequence validation of two single cell clones. **e**, Western blotting

of nucleoplasm and chromatin fractions from two MTF2-knockout clones and control cells. Data are representative of two independent experiments. **f, g**, RT-qPCR of control cells and two MTF2-knockout clones (**f**) or control, knockout, or MTF2-knockout cells rescued with wild-type or MTF2(Lys339Ala) (**g**). Data are mean  $\pm$  s.d. of three biological replicates. **h**, ChIP-qPCR experiments in control, MTF2-knockout, and rescued cells with the antibodies shown. Data are mean  $\pm$  s.d. of two biological replicates. Uncropped blots are shown in Supplementary Fig. 1.



**Extended Data Figure 5 | Analysis of the ChIP-seq experiments and PHF19-knockdown ChIP-seq data.** **a**, Comparison of normalized ChIP-seq promoter reads (as in Fig. 4f) of three biological replicates for MTF2, SUZ12 and H3K27me3. The whisker-box plots represent the lower quartile, median and upper quartile of the data with 5% and 95% whiskers.

**b**, Comparison of MTF2 ChIP-seq data in control and MTF2-knockout cells (replicate 3) at the three promoter groups described in Fig. 4a. **c**, Promoter profiles of SUZ12 and H3K27me3 in control and PHF19-knockdown cells using publically available data<sup>10</sup>.



**Extended Data Figure 6 | EMSA and HMTase experiments with purified MTF2-PRC2 complex.** **a**, Silver staining of purified wild-type or Lys339Ala mutant human MTF2-PRC2 complexes (and mock control) from HeLa-S cells. F/H, Flag-HA-tagged. **b**, Western blotting of the eluates from **a**. **c**, EMSA experiment with equal volumes (0, 0.5, 1, 2, 3  $\mu$ l) of the eluates using the 12-mer-CpG sequence. Data are representative of two independent experiments. **d**, Histone methyltransferase (HMTase) experiment using equal volumes (15  $\mu$ l) of the eluates from **a**. Two technical replicates are shown. H3K27me3 levels were investigated by western blotting. Uncropped blots are shown in Supplementary Fig. 1.

**Extended Data Table 1 | X-ray statistics of the PHF1 and MTF2 Tudor-PHD1-PHD2-EH cassettes in the free or DNA- and/or histone-bound states**

## Data collection and refinement statistics

Crystal	Free human PHF1 (26-340) form 1	Free human PHF1 (26-340) form 2	Human PHF1 (26-360) and DNA complex	Human MTF2 (42-358) with DNA and H3(33-40)K36me3	Mouse PHF1(26-360) with DNA and H3(29-41)K36me3
Beam line	APS-19ID	APS-19ID	SSRF-BL18U1	SSRF-BL19U1	SSRF-BL19U1
Wavelength	0.97918	0.97918	0.97791	0.97853	0.97852
Space group	<i>P</i> 2 <sub>1</sub> 2 <sub>1</sub> 2 <sub>1</sub>	<i>P</i> 2 <sub>1</sub> 2 <sub>1</sub> 2 <sub>1</sub>	<i>P</i> 2 <sub>1</sub> 2 <sub>1</sub> 2	<i>P</i> 3 <sub>1</sub> 2	<i>C</i> 2
Unit cell a, b, c (Å)	40.0, 62.0, 135.4	61.5, 66.8, 76.2	109.6, 110.3, 118.9	137.7, 137.7, 101.2	141.2, 62.6, 97.3
Unit cell $\alpha$ , $\beta$ , $\gamma$ (°)	90.0, 90.0, 90.0	90.0, 90.0, 90.0	90.0, 90.0, 90.0	90.0, 90.0, 120.0	90.0, 108.0, 90.0
Resolution (Å)	36.49-1.90 (1.96-1.90) <sup>a</sup>	29.34-1.90 (1.96-1.90)	50.0-2.30 (2.34-2.30)	50.0-2.25 (2.30-2.25)	50.0-2.40 (2.46-2.40)
R <sub>sym</sub>	0.135 (0.849)	0.132 (0.807)	0.123 (0.820)	0.124 (0.894)	0.086 (0.485)
I/ $\sigma$ (I)	16.6 (1.9)	18.8 (2.5)	22.4 (2.0)	19.6 (3.0)	17.9 (1.8)
Completeness (%)	97.3 (96.7)	100 (100)	99.9 (100)	100 (100)	99.1 (99.1)
Redundancy	4.7 (4.3)	6.6 (6.1)	9.2 (9.3)	16.9 (17.4)	3.6 (3.3)
Unique reflections	126328	171303	65188	52840	32456
R <sub>work</sub> /R <sub>free</sub> (%)	18.3/21.8	17.7/22.7	20.9/24.4	20.1/23.1	22.2/25.7
Number of non-H atoms					
Protein	2397	2509	7290	4979	5031
DNA	0	0	526	526	506
Water	183	203	190	331	56
ligands	4	4	28	8	8
Average B factors (Å <sup>2</sup> )					
Protein	27.9	24.7	62.1	38.9	57.8
DNA	no	no	58.6	41.0	72.1
Water	18.5	21.0	50.1	38.4	51.4
Other ligands	32.4	31.2	24.5	38.6	59.6
R.m.s. deviations					
Bond lengths (Å)	0.007	0.007	0.003	0.003	0.005
Bond angles (°)	0.998	1.04	0.641	0.634	0.793

<sup>a</sup> Highest resolution shell (in Å) shown in parentheses.

**Extended Data Table 2 | ITC-based binding affinity measurements for the PCL cassettes or their mutants with DNAs or histones**

DNA or peptide	Protein Sample	$K_d$ ( $\mu$ M)	$\Delta H$ (cal/mol)
12-mer-CpG	PHF1 (26-360)	$1.2 \pm 0.3$	$-3608 \pm 97$
12-mer-CpG	PHF1 (165-360)	$0.5 \pm 0.1$	$-5457 \pm 88$
12-mer-ACpGG	PHF1 (165-360)	NB	
12-mer-TCpGG	PHF1 (165-360)	$0.8 \pm 0.4$	$-1170 \pm 80$
12-mer-CCpGG	PHF1 (165-360)	$22 \pm 4$	$4516 \pm 467$
12-mer-GCpGA	PHF1 (165-360)	$31 \pm 2$	$4422 \pm 207$
12-mer-GCpGT	PHF1 (165-360)	$3.9 \pm 0.5$	$-3053 \pm 117$
14-mer-GCpGC	PHF1 (165-360)	$11.3 \pm 0.8$	$-4281 \pm 125$
12-mer-ACpGA	PHF1 (165-360)	NB	
12-mer-ACpGT	PHF1 (165-360)	NB	
12-mer-TCpGA	PHF1 (165-360)	NB	
H3(29-43)K36me3	PHF1 (26-360)	$2.0 \pm 0.1$	$-9826 \pm 62$
H3(21-33)K27me3	PHF1 (26-360)	$50 \pm 7$	$-5970 \pm 433$
H3(29-43)K36me3/R40A	PHF1 (26-360)	$5.2 \pm 0.3$	$-8169 \pm 70$
H3(1-15)K4me3	PHF1 (26-360)	$215 \pm 38$	$-8712 \pm 2195$
H3(29-43)	PHF1 (26-360)	NB	
H3(1-15)	PHF1 (26-360)	NB	
H3(29-43)K36me3	PHF1 (26-360)-Y47A	NB	
12-mer-CpG	MTF2 (180-378)	$2.1 \pm 0.3$	$-1767 \pm 44$
12-mer-ACpGG	MTF2 (180-378)	$33 \pm 6$	$5836 \pm 1100$
12-mer-TCpGG	MTF2 (180-378)	$6.4 \pm 1.0$	$2373 \pm 106$
12-mer-CCpGG	MTF2 (180-378)	$12 \pm 1$	$5831 \pm 99$
12-mer-GCpGA	MTF2 (180-378)	$22 \pm 7$	$3762 \pm 922$
12-mer-GCpGT	MTF2 (180-378)	$25 \pm 4$	$3927 \pm 292$
14-mer-GCpGC	MTF2 (180-378)	$9 \pm 2$	$2924 \pm 220$
12-mer-ACpGA	MTF2 (180-378)	NB	
12-mer-ACpGT	MTF2 (180-378)	NB	
12-mer-TCpGA	MTF2 (180-378)	NB	
H3(29-43)K36me3	MTF2 (42-378)	$45 \pm 5$	$-3380 \pm 306$
H3(21-33)K27me3	MTF2 (42-378)	NB	
H3(29-43)	MTF2 (42-378)	NB	
H3(29-43)K36me3	MTF2 (42-378)-Y62A	NB	
NB, no detectable binding			

**Extended Data Table 3 | Names and sequences of the double-stranded DNAs used**

DNA name	DNA sequence
WH motif	CTATGTAAACAAC
16-mer-AT-rich	TTTTTATTAATAAAAA
12-mer-CpG	GGCGGCCGCC
12-mer-GpC	GGGGGGCCCC
12-mer-ApG	GGGAGGCCTCCC
12-mer-TpG	GGGTGGCCACCC
12-mer-CpA	GGCAGCTGCC
12-mer-CpT	GGGCTGCAGCCC
12-mer-CpC	GGCCTAGGCC
12-mer-ACpGG	GGACGGCCGTCC
12-mer-TCpGG	GGTCGGCCGACC
12-mer-CCpGG	GGCCGGCCGGCC
12-mer-GCpGA	GGCGATCGCCC
12-mer-GCpGT	GGCGTACGCC
14-mer-GCpGC	GGCGCTAGCGCCC
12-mer-ACpGA	GGACGATCGTCC
12-mer-ACpGT	GGACGTACGTCC
12-mer-TCpGA	GGTCGATCGACC
12-mer-CpG-m1	GGC(m)GGCCGCC
12-mer-CpG-m2	GGC(m)GGCC(m)GCC

For each DNA duplex, only the sequence of one strand is listed in the table. Cytosine methylation is labelled as (m).

Extended Data Table 4 | Primers used for ChIP-qPCR and RT-qPCR

Target genes	Forward primer sequences	Reverse primer sequences
<b>CHIP-qPCR</b>		
<i>Otx1</i>	AGTAGGCGTGCTCAGAGAGG	GGCCGGTCAAGAAGAAGTC
<i>Hoxb3</i>	CCGTGCGATGAAGTACAAGA	CCTTAAGAGGGGGCTGGTAG
<i>Hoxa10</i>	CTTTTGCAGCAGAACATCAAA	GTAGCCGGGTACTGGCACT
<i>Nkx2-9</i>	TGGCACCTTCCGGACTTG	AAGTGCGAGGCGCTCG
<i>Msx1</i>	ACAGAAAGAAATAGCACAGACCATAAGA	TTCTACCAAGTTCAGAGGGACTTT
<i>Hoxa7</i>	GAGAGGTGGGCAAAGAGTGG	CCGACAACCTCATACCTATTCTG
<i>Pou5f1</i>	GGCTCTCCAGAGGATGGCTGAG	TCCGATGCCCCATCGCA
<i>Sox2</i>	CCATCCACCCTTATGTATCCAAG	CGAAGGAAGTGGGTAAACAGCAC
<b>RT-qPCR</b>		
<i>Mtf2</i> (1)	ATGAGAGACTCTACAGGAGCAG	GCTAAGACATCTTGACCCTCTTC
<i>Mtf2</i> (2)	CAGATGAAAAGTGGCTTTGTCTG	TGCATCCCATTCAAGGTCAGC
<i>Tbx1</i>	CTGTGGGACGAGTTCAATCAG	TTGTCATCTACGGGCACAAAG
<i>Gata4</i>	CACAAGATGAACGGCATCAACC	CAGCGTGGTGGTGGTAGTCTG
<i>Pax2</i>	AAGCCCGGAGTGATTGGTG	CAGGCGAACATAGTCGGGTT
<i>Pax3</i>	TCCCATGGTTGCGTCTCTAAG	CTCCACGTCAGGCGTTGTC
<i>Pax5</i>	CCATCAGGACAGGACATGGAG	GGCAAGTTCCTACTATCCTTTGG
<i>Six1</i>	ATGCTGCCGTCGTTTGGTT	CCTTGAGCACGCTCTCGTT
<i>Hoxc13</i>	GCCGTCTACACGGACATCC	CCCCAAATGGGTAACCATAGC
<i>Msx1</i>	TGCTGCTATGACTTCTTTGCC	GCTTCTGTGATCGGCCAT
<i>Msx3</i>	ACCCTCCGCAAACACAAAAC	CGCTCCGCAATGGATAAGTAT
<i>Hoxa10</i>	CCTGCCGCGAACTCCTTTT	GGCGCTTCATTACGCTTGC
<i>Nkx1-2</i>	CGCTCTGCCCTATCAGACTTT	GGCCCAAGGAATGGAGTGA
<i>Meis1</i>	GCAAAGTATGCCAGGGGAGTA	TCCTGTGTTAAGAACCGAGGG
<i>Pou5f1</i>	AGAGGATCACCTTGGGGTACA	CGAAGCGACAGATGGTGGTC
<i>Nanog</i>	CACAGTTTGCCTAGTTCTGAGG	GCAAGAATAGTTCTCGGGATGAA
<i>Sox2</i>	GCGGAGTGAAACTTTTGTC	GGGAAGCGTGACTTATCCTTCT
<i>Esrrb</i>	GGACTCGCCGCTATGTTCT	CGTTAAGCATGTACTCGCATTTG
<i>Tet1</i>	GCAGTGAACCCCGAAAAC	AGAGCCATTGTAAACCCGTTG
<i>Zbtb7a</i>	CTTTGCGACGTGGTGATTCTT	CGTTCTGCTGGTCCACTACA

## Life Sciences Reporting Summary

Nature Research wishes to improve the reproducibility of the work that we publish. This form is intended for publication with all accepted life science papers and provides structure for consistency and transparency in reporting. Every life science submission will use this form; some list items might not apply to an individual manuscript, but all fields must be completed for clarity.

For further information on the points included in this form, see [Reporting Life Sciences Research](#). For further information on Nature Research policies, including our [data availability policy](#), see [Authors & Referees](#) and the [Editorial Policy Checklist](#).

### ▶ Experimental design

#### 1. Sample size

Describe how sample size was determined.

No statistical methods were used to predetermine sample size.

#### 2. Data exclusions

Describe any data exclusions.

No

#### 3. Replication

Describe whether the experimental findings were reliably reproduced.

All experimental findings could reliable be reproduced.

#### 4. Randomization

Describe how samples/organisms/participants were allocated into experimental groups.

The experiments were not randomized.

#### 5. Blinding

Describe whether the investigators were blinded to group allocation during data collection and/or analysis.

Investigators were not blinded to allocation during experiments and outcome assessment.

Note: all studies involving animals and/or human research participants must disclose whether blinding and randomization were used.

#### 6. Statistical parameters

For all figures and tables that use statistical methods, confirm that the following items are present in relevant figure legends (or in the Methods section if additional space is needed).

- |                                     |  |
|-------------------------------------|--|
| n/a                                 | Confirmed  |
| <input checked="" type="checkbox"/> | <input type="checkbox"/> The <u>exact sample size</u> ( $n$ ) for each experimental group/condition, given as a discrete number and unit of measurement (animals, litters, cultures, etc.)   |
| <input type="checkbox"/>            | <input checked="" type="checkbox"/> A description of how samples were collected, noting whether measurements were taken from distinct samples or whether the same sample was measured repeatedly   |
| <input type="checkbox"/>            | <input checked="" type="checkbox"/> A statement indicating how many times each experiment was replicated   |
| <input type="checkbox"/>            | <input checked="" type="checkbox"/> The statistical test(s) used and whether they are one- or two-sided (note: only common tests should be described solely by name; more complex techniques should be described in the Methods section) |
| <input type="checkbox"/>            | <input checked="" type="checkbox"/> A description of any assumptions or corrections, such as an adjustment for multiple comparisons  |
| <input type="checkbox"/>            | <input checked="" type="checkbox"/> The test results (e.g. $P$ values) given as exact values whenever possible and with confidence intervals noted   |
| <input type="checkbox"/>            | <input checked="" type="checkbox"/> A clear description of statistics including <u>central tendency</u> (e.g. median, mean) and <u>variation</u> (e.g. standard deviation, interquartile range)  |
| <input type="checkbox"/>            | <input checked="" type="checkbox"/> Clearly defined error bars   |

See the web collection on [statistics for biologists](#) for further resources and guidance.

## ► Software

Policy information about [availability of computer code](#)

### 7. Software

Describe the software used to analyze the data in this study.

Bowtie 1.0, Tophat 2.1.0, Cuffdiff 2.2.1.3, DeepTools/BamCoverage 2.3.6.0, Cistrome, MACS 1.0, R 3.3.1, FastQC 0.11.3, HKL2000, COOT, PHENIX, Pymol

For manuscripts utilizing custom algorithms or software that are central to the paper but not yet described in the published literature, software must be made available to editors and reviewers upon request. We strongly encourage code deposition in a community repository (e.g. GitHub). *Nature Methods* [guidance for providing algorithms and software for publication](#) provides further information on this topic.

## ► Materials and reagents

Policy information about [availability of materials](#)

### 8. Materials availability

Indicate whether there are restrictions on availability of unique materials or if these materials are only available for distribution by a for-profit company.

Unique materials are available from authors upon request.

### 9. Antibodies

Describe the antibodies used and how they were validated for use in the system under study (i.e. assay and species).

SUZ12 (Western) (Santa Cruz, sc-46264, Western), SUZ12 (D39F6, Cell Signaling, ChIP), Actin (abcam, ab3280), Histone H3 (abcam, ab1791), H3K27me3 (Millipore, 07-449), H3K4me3 (Millipore, 04-745), MTF2 (Proteintech, 16208-1-AP). All antibodies were validated by Western blotting using mouse embryonic stem cells.

### 10. Eukaryotic cell lines

a. State the source of each eukaryotic cell line used.

E14TG2a cells were obtained of ATCC

b. Describe the method of cell line authentication used.

Cells were not authenticated

c. Report whether the cell lines were tested for mycoplasma contamination.

Cell line was negatively tested for mycoplasma

d. If any of the cell lines used are listed in the database of commonly misidentified cell lines maintained by [ICLAC](#), provide a scientific rationale for their use.

Not applicable

## ► Animals and human research participants

Policy information about [studies involving animals](#); when reporting animal research, follow the [ARRIVE guidelines](#)

### 11. Description of research animals

Provide details on animals and/or animal-derived materials used in the study.

Not applicable

Policy information about [studies involving human research participants](#)

### 12. Description of human research participants

Describe the covariate-relevant population characteristics of the human research participants.

Not applicable

## ChIP-seq Reporting Summary

Form fields will expand as needed. Please do not leave fields blank.

### ▶ Data deposition

1. For all ChIP-seq data:

- a. Confirm that both raw and final processed data have been deposited in a public database such as [GEO](#).
- b. Confirm that you have deposited or provided access to graph files (e.g. BED files) for the called peaks.

2. Provide all necessary reviewer access links.

*The entry may remain private before publication.*

<https://www.ncbi.nlm.nih.gov/geo/query/acc.cgi?token=kbazmoaedjyrlwf&acc=GSE97805>

3. Provide a list of all files available in the database submission.

MTF2-Control-Repl1.fastq.gz  
 MTF2-MTF2KO-Repl1.fastq.gz  
 MTF2-RescueWT-Repl1.fastq.gz  
 MTF2-RescueK339A-Repl1.fastq.gz  
 MTF2-Control-Repl2.fastq.gz  
 MTF2-MTF2KO-Repl2.fastq.gz  
 MTF2-RescueWT-Repl2.fastq.gz  
 MTF2-RescueK339A-Repl2.fastq.gz  
 SUZ12-Control-Repl1.fastq.gz  
 SUZ12-MTF2KO-Repl1.fastq.gz  
 SUZ12-RescueWT-Repl1.fastq.gz  
 SUZ12-RescueK339A-Repl1.fastq.gz  
 SUZ12-Control-Repl2.fastq.gz  
 SUZ12-MTF2KO-Repl2.fastq.gz  
 SUZ12-RescueWT-Repl2.fastq.gz  
 SUZ12-RescueK339A-Repl2.fastq.gz  
 H3K27me3-Control-Repl1.fastq.gz  
 H3K27me3-MTF2KO-Repl1.fastq.gz  
 H3K27me3-RescueK339A-Repl1.fastq.gz  
 H3K27me3-RescueWT-Repl1.fastq.gz  
 H3K27me3-Control-Repl2.fastq.gz  
 H3K27me3-MTF2KO-Repl2.fastq.gz  
 H3K27me3-RescueWT-Repl2.fastq.gz  
 H3K27me3-RescueK339A-Repl2.fastq.gz  
 MTF2-Control-Repl3.fastq.gz  
 MTF2-MTF2KO-Repl3.fastq.gz  
 MTF2-RescueWT-Repl3.fastq.gz  
 MTF2-RescueK339A-Repl3.fastq.gz  
 SUZ12-Control-Repl3.fastq.gz  
 SUZ12-MTF2KO-Repl3.fastq.gz  
 SUZ12-RescueWT-Repl3.fastq.gz  
 SUZ12-RescueK339A-Repl3.fastq.gz  
 H3K27me3-Control-Repl3.fastq.gz  
 H3K27me3-MTF2KO-Repl3.fastq.gz  
 H3K27me3-RescueWT-Repl3.fastq.gz  
 H3K27me3-RescueK339A-Repl3.fastq.gz  
 Input.fastq.gz  
 MTF2-Control-Repl1-mm9.bigwig  
 MTF2-MTF2KO-Repl1-mm9.bigwig  
 MTF2-RescueWT-Repl1-mm9.bigwig

MTF2-RescueK339A-Repl1-mm9.bigwig  
 MTF2-Control-Repl2-mm9.bigwig  
 MTF2-MTF2KO-Repl2-mm9.bigwig  
 MTF2-RescueWT-Repl2-mm9.bigwig  
 MTF2-RescueK339A-Repl2-mm9.bigwig  
 SUZ12-Control-Repl1-mm9.bigwig  
 SUZ12-MTF2KO-Repl1-mm9.bigwig  
 SUZ12-RescueWT-Repl1-mm9.bigwig  
 SUZ12-RescueK339A-Repl1-mm9.bigwig  
 SUZ12-Control-Repl2-mm9.bigwig  
 SUZ12-MTF2KO-Repl2-mm9.bigwig  
 SUZ12-RescueWT-Repl2-mm9.bigwig  
 SUZ12-RescueK339A-Repl2-mm9.bigwig  
 H3K27me3-Control-Repl1-mm9.bigwig  
 H3K27me3-MTF2KO-Repl1-mm9.bigwig  
 H3K27me3-RescueWT-Repl1-mm9.bigwig  
 H3K27me3-RescueK339A-Repl1-mm9.bigwig  
 H3K27me3-Control-Repl2-mm9.bigwig  
 H3K27me3-MTF2KO-Repl2-mm9.bigwig  
 H3K27me3-RescueWT-Repl2-mm9.bigwig  
 H3K27me3-RescueK339A-Repl2-mm9.bigwig  
 MTF2-Control-Repl3-mm9.bigwig  
 MTF2-MTF2KO-Repl3-mm9.bigwig  
 MTF2-RescueWT-Repl3-mm9.bigwig  
 MTF2-RescueK339A-Repl3-mm9.bigwig  
 MTF2-Control-Repl1-3combined-mm9.bigwig  
 MTF2-MTF2KO-Repl1-3combined-mm9.bigwig  
 MTF2-RescueWT-Repl1-3combined-mm9.bigwig  
 MTF2-RescueK339A-Repl1-3combined-mm9.bigwig  
 SUZ12-Control-Repl3-mm9.bigwig  
 SUZ12-MTF2KO-Repl3-mm9.bigwig  
 SUZ12-RescueWT-Repl3-mm9.bigwig  
 SUZ12-RescueK339A-Repl3-mm9.bigwig  
 SUZ12-Control-Repl1-3combined-mm9.bigwig  
 SUZ12-MTF2KO-Repl1-3combined-mm9.bigwig  
 SUZ12-RescueWT-Repl1-3combined-mm9.bigwig  
 SUZ12-RescueK339A-Repl1-3combined-mm9.bigwig  
 H3K27me3-Control-Repl3-mm9.bigwig  
 H3K27me3-MTF2KO-Repl3-mm9.bigwig  
 H3K27me3-RescueWT-Repl3-mm9.bigwig  
 H3K27me3-RescueK339A-Repl3-mm9.bigwig  
 H3K27me3-Control-Repl1-3combined-mm9.bigwig  
 H3K27me3-MTF2KO-Repl1-3combined-mm9.bigwig  
 H3K27me3-RescueWT-Repl1-3combined-mm9.bigwig  
 H3K27me3-RescueK339A-Repl1-3combined-mm9.bigwig  
 Input-mm9.bigwig

4. If available, provide a link to an anonymized genome browser session (e.g. [UCSC](#)).

not available

## ► Methodological details

5. Describe the experimental replicates.

ChIP-Seq for MTF2, SUZ12 and H3K27me3 in Control, MTF2 KO, Rescue MTF2 wildtype and Rescue MTF2 K339A, in three biological replicates

6. Describe the sequencing depth for each experiment.

Experiment TotalReads Uniquely Mapped Reads  
 MTF2-Control Repl1 11395234 7527065  
 MTF2-MTF2KO2 Repl1 15400800 10051717  
 MTF2-RescueWT Repl1 12800228 3276512  
 MTF2-RescueK339A Repl1 14403676 9064199

MTF2-Control Repl2 22754287 16043248  
 MTF2-MTF2KO2 Repl2 18218612 12444818  
 MTF2-RescueWT Repl2 18847954 1247134  
 MTF2-RescueK339A Repl2 13667870 9367468  
 MTF2-Control Repl3 18681217 9224426  
 MTF2-MTF2KO2 Repl3 24788217 10541430  
 MTF2-RescueWT Repl3 18564441 8520077  
 MTF2-RescueK339A Repl3 24851782 10983653  
 SUZ12-Control Repl1 30064447 20165629  
 SUZ12-MTF2KO2 Repl1 22278689 15122739  
 SUZ12-RescueWT Repl1 21654164 13912968  
 SUZ12-RescueK339A Repl1 16961501 10723543  
 SUZ12-Control Repl2 13972559 9559860  
 SUZ12-MTF2KO2 Repl2 13142947 8685050  
 SUZ12-RescueWT Repl2 14951380 10176807  
 SUZ12-RescueK339A Repl2 14820007 10194611  
 SUZ12-Control Repl3 27786100 16189659  
 SUZ12-MTF2KO2 Repl3 27274028 14896663  
 SUZ12-RescueWT Repl3 28342823 13263028  
 SUZ12-RescueK339A Repl3 22334148 11229513  
 H3K27me3-Control Repl1 10832725 6892870  
 H3K27me3-MTF2KO2 Repl1 12925881 8493457  
 H3K27me3-RescueWT Repl1 24991145 15180001  
 H3K27me3-RescueK339A Repl1 17121836 10606241  
 H3K27me3-Control Repl2 34011614 2330482  
 H3K27me3-MTF2KO2 Repl2 12495747 7851959  
 H3K27me3-RescueWT Repl2 14532355 9739975  
 H3K27me3-RescueK339A Repl2 14023765 9450662  
 H3K27me3-Control Repl3 25524374 12358458  
 H3K27me3-MTF2KO2 Repl3 26758792 13749136  
 H3K27me3-RescueWT Repl3 22356569 11062096  
 H3K27me3-RescueK339A Repl3 24478134 11453088  
 Input 18904628 12472723

7. Describe the antibodies used for the ChIP-seq experiments.

MTF2: 16208-1-AP, ProteinTech  
 SUZ12: D39F6, Cell Signaling  
 H3K27me3: 07-449, Millipore

8. Describe the peak calling parameters.

MACS,  $p < 1e-05$

9. Describe the methods used to ensure data quality.

FastQC

10. Describe the software used to collect and analyze the ChIP-seq data.

Bowtie, DeepTools, Cistrome and R